



This is a repository copy of *Application of Raman spectroscopy to real-time monitoring of CO2 capture at PACT pilot plant; Part 1: Plant operational data.*

White Rose Research Online URL for this paper:
<http://eprints.whiterose.ac.uk/155636/>

Version: Accepted Version

Article:

Akram, M., Jinadasa, W., Tait, P. et al. (6 more authors) (2020) Application of Raman spectroscopy to real-time monitoring of CO2 capture at PACT pilot plant; Part 1: Plant operational data. *International Journal of Greenhouse Gas Control*, 95. 102969. ISSN 1750-5836

<https://doi.org/10.1016/j.ijggc.2020.102969>

Article available under the terms of the CC-BY-NC-ND licence
(<https://creativecommons.org/licenses/by-nc-nd/4.0/>).

Reuse

This article is distributed under the terms of the Creative Commons Attribution-NonCommercial-NoDerivs (CC BY-NC-ND) licence. This licence only allows you to download this work and share it with others as long as you credit the authors, but you can't change the article in any way or use it commercially. More information and the full terms of the licence here: <https://creativecommons.org/licenses/>

Takedown

If you consider content in White Rose Research Online to be in breach of UK law, please notify us by emailing eprints@whiterose.ac.uk including the URL of the record and the reason for the withdrawal request.



eprints@whiterose.ac.uk
<https://eprints.whiterose.ac.uk/>

Application of Raman Spectroscopy to Real-Time Monitoring of CO₂ Capture at PACT pilot Plant; Part 1: Plant operational data

Muhammad Akram^{a,*}, M.H. Wathsala N. Jinadasa^b, Paul Tait^c, Mathieu Lucquiaud^c, Kris Milkowski^a, Janos Szuhanszki^a, Klaus-Joachim Jens^b, Maths Halstensen^b, Mohammed Pourkashanian^a,

^aThe University of Sheffield, United Kingdom

^bUniversity of South-eastern Norway, Norway

^cThe University of Edinburgh, United Kingdom

*Corresponding author: m.akram@sheffield.ac.uk

Energy2050, Energy Engineering Group, Department of Mechanical Engineering, Ella Armitage Building, University of Sheffield, Sheffield S3 7RD, UK

ABSTRACT

Process analyzers for in-situ monitoring give advantages over the traditional analytical methods such as their fast response, multi-chemical information from a single measurement unit, minimal errors in sample handling and ability to use for process control. This study discusses the suitability of Raman spectroscopy as a process analytical tool for in-situ monitoring of CO₂ capture using aqueous monoethanolamine (MEA) solution by presenting its performance during a 3-day test campaign at PACT pilot plant in Sheffield, UK. Two Raman immersion probes were installed on lean and rich streams for real time measurements. A multivariate regression model was used to determine the CO₂ loading. The plant performance is described in detail by comparing the CO₂ loading in each solvent stream at different process conditions. The study shows that the predicted CO₂ loading recorded an acceptable agreement with the offline measurements. The findings from this study suggest that Raman Spectroscopy has the capability to follow changes in process variables and can be employed for real time monitoring and control of the CO₂ capture process. In addition, these predictions can be used to optimize process parameters; to generate data to use as inputs for thermodynamic models, plant design and scale-up scenarios.

Keywords : CO₂ capture, Raman spectroscopy, in-situ process monitoring

1. Introduction

Carbon Capture, Utilisation and Storage (CCUS) is gaining highlights due to its potential to tackle the climate change problem. The UK Government's "Clean Growth Strategy" highlights the role of CCUS in reducing greenhouse gas emissions alongside other options i.e. the need for switching from fossils to low carbon fuels (Clean Growth, 2018). Although the technology is expensive at the moment, it has the potential to provide deep and affordable CO₂ emission reductions from coal and gas-fired power generation. The technologies to meet greenhouse gas emission limits will cost double if no CCUS is used (BEIS report, 2019). There are many technological options being considered for CCUS but post combustion capture using alkanolamine solutions is by far the most understood process due its long time use in the process industry. Although this process has been applied in the oil and gas industry for many decades (Polasek and Bullin, 2006), it has been predominantly applied to clean gases. Its application to

42 power plant and industrial flue gases, which may have contaminants, is relatively new and is in
43 the early phase of commercial deployment. Sask Power (Boundary Dam 3) in Canada and Petra
44 Nova in USA are two example of commercial deployment of this versatile technology. There
45 are also a number of research facilities in industrial and academic setups working on different
46 aspects of the technology (de Cazenove et al. 2016; Akram et al. 2016; Notz et al. 2012; Mejdell
47 et al. 2011).

48 Several research work is carried on developing and optimizing methods to remove CO₂ from
49 power plants and industrial sources using amine technology. Process modifications (Kang et al.
50 2016; Jassim et al. 2007; Le Moullec et al. 2014; Madan et al. 2013; Ahn et al. 2013; Amrollahi
51 et al. 2011; Oh et al. 2018; Diego et al. 2017; Merkel et al. 2013; Herraiz, 2016) and new
52 solvents (Aronu et al. 2010; Kumar et al. 2014; Hakka 2007; Yuan and Rochelle, 2018; Wang
53 et al. 2015; Yang et al. 2016; Kim et al. 2013; Cheng et al. 2013; Abu Zahra et al. 2007) are
54 being tested to minimise these issues. The process is complex and is greatly affected by process
55 parameters. Moreover, the presence of oxygen and other impurities such as NO_x and SO_x in the
56 flue gases cause solvent degradation. Degraded solvent results in reduced process performance.
57 Inline solvent monitoring is essential for real-time evaluation of the plant performance and
58 assessing solvent quality. Moreover, it is an important aspect from solvent management point
59 of view and in order to control the process at optimum conditions. However, a well-established
60 method for this purpose is currently not available.

61 The chemical process of CO₂ absorption by aqueous MEA solutions are attributed by a number
62 of parameters including CO₂ loading (mol_{CO2}/mol_{MEA}) and solvent concentration. The CO₂
63 loading in an absorption process is also an indication of the carbon species-products that exist
64 as a result of the reaction between CO₂ with amine while in a desorption process it expresses
65 the efficiency of desorption and degree of regeneration of the solvent for the recirculation to
66 the absorption column for further CO₂ capture from flue gas. Solvent concentration can vary
67 during the process due to evaporative and degradation losses. The solvent concentration has to
68 be maintained for optimum operation of CO₂ capture plants. Therefore these two parameters
69 are frequently tested during plant operations to characterize both absorption and desorption
70 while a detailed analysis of all the chemical components in the solvent stream is important to
71 understand chemical mechanisms and reaction kinetics. It is apparent that a real-time
72 measurement represents actual plant operation more realistically than a periodical monitoring
73 method which only gives measurements in different time intervals where the non-measured
74 points are predicted based on the trend which can lead to either over-predictions or under-
75 predictions. Unavailability of real-time measurements results in lack of process control. The
76 CO₂ capture process by amines needed to be improved and optimized, to reduce the capital and
77 operational cost and find solutions for amine degradation and corrosion problems. Availability
78 of a real-time monitoring method will provide increased process understanding and possible
79 routes of continuous improvement in a faster and more reliable way. In addition, real-time
80 monitoring helps for making more data-driven decisions.

81 Few developments are published in real-time monitoring methods of CO₂ capture process.
82 Monitoring of CO₂ capture by aqueous AMP-PZ system and MDEA-PZ high pressure system
83 are reported by TNO group, Netherlands using chemometrics approach and pilot plant
84 demonstration. They predicted the concentrations of MDEA, PZ, and CO₂ using real-time
85 measurements of solvent properties which were density, pH, conductivity, sound velocity,
86 refractive index and NIR absorption (Kachko *et al.*, 2016a). A similar approach was used to
87 predict AMP, PZ and CO₂ in another pilot plant test (Kachko et al., 2015). During long term
88 pilot demonstrations at TCM CO₂ capture pilot plant in Norway, CO₂ loadings and solvent
89 concentration were mainly followed on a daily basis with manual samples and analysis and they
90 also used online analyzers such as conductivity, density and pH to make correlations to CO₂

91 loading and solvent strength (Andersson *et al.*, 2013; Flø *et al.*, 2017; Montañés *et al.*, 2017).
92 Due to the long term use and proven reliability, and familiarity with wet chemical methods,
93 offline analysis are still used such as barium chloride (BaCl₂) titration-precipitation method
94 (Idris *et al.*, 2014; Weiland *et al.*, 1969) and analysis via acidic evolution (Hilliard, 2008) and
95 LC-MS (Knudsen *et al.*, 2014) for determining CO₂ loadings.

96
97 Raman spectroscopy is one of in-situ monitoring tools in manufacturing industry. It gives
98 unique data based on the Raman scattered light by laser induced molecular vibrations. It
99 provides a high information content about a chemical system, faster measurements within few
100 seconds, no sample preparation is required and easy to use in plant applications. A method for
101 in situ specie distribution of a CO₂ loaded alkanolamine solution by Raman spectroscopy was
102 proposed by (Souchon *et al.*, 2011) and (Vogt *et al.*, 2011) showed how CO₂ loading can be
103 qualitatively interpreted from Raman spectra. A complete carbon and amine specie distribution
104 was presented by (Wong *et al.*, 2015, 2016). Samarakoon *et al.*, (2013) proposed a method to
105 determine carbon species in a CO₂ loaded MEA solution by calculating molar scattering factor
106 while (Idris *et al.*, 2014) used area under a Raman peak to develop calibration curves. Raman
107 spectroscopy for real-time quantitative analysis was demonstrated in a laboratory rig operation
108 for MEA solvent by Jinadasa *et al.*, (2017). A comparison of Raman method with infrared
109 spectroscopy was presented by Puxty *et al.*, (2016) while Kachko *et al.*, (2016b) compared
110 Raman, near infrared, and Fourier-transform infrared for in-line monitoring of CO₂ capture
111 plants. The above cited literature reveals the capability of Raman method for monitoring the
112 concentration profiles in real-time applications.

113
114 There is not much published data on the use of Raman Spectroscopy as a real time plant
115 monitoring and optimization tool. This study supports the use of this technique in two aspects.
116 Firstly, it demonstrates the reliability of the spectroscopic method for faster and precise
117 measurements in a variety of process conditions by comparing the Raman measurements with
118 standard offline analytical results. Secondly, it provides evidence for the response of CO₂
119 absorption and desorption process on steady and dynamic process conditions and its sensitivity
120 thus proving the capability of Raman spectroscopy to be used as a tool to increase process
121 understanding, optimization and control. Trials for this study were performed as a three day-
122 campaign at UKCCSRC Pilot-scale Advanced CO₂ Capture Technology (PACT) Facility,
123 Sheffield, UK. The trends in key plant variables capture efficiency, temperature profiles and
124 emission measurements are presented and discussed with respect to Raman measurements. To
125 the author's knowledge, in open literature, no one has analyzed the capture process performance
126 with parametric changes in relation to Raman Spectroscopy measurements in as detail as
127 presented in this paper.

128 A Raman measurement is a spectrum which shows the Raman scattering intensity as a function
129 of the frequency shifts. This intensity depends on the vibrational, rotational and other low
130 frequency transitions in molecules when excited by a laser. Calibration is required to convert
131 the indirect Raman measurement into a useful information such as a concentration of chemical
132 specie in a system. There are two types of calibration approaches which are univariate analysis
133 and multivariate analysis. A chemometric based multivariate approach was used in this study
134 to convert raw Raman spectra into concentration values because this method is more robust
135 than the traditional univariate analysis (Esbensen, 2010). The process of instrument calibration
136 to fit for a plant operation is an extensive process and therefore is presented as the second part
137 of this paper in a different publication titled as "Raman Spectroscopy for Real-Time Monitoring
138 of CO₂ Capture Process; Part 2: Multivariate Calibration".

139 2. Methodology

140 2.1. Description of CO₂ capture pilot plant

141 The PACT Core Facilities in Sheffield, UK is intended for commercial and academic research
142 enabling users to develop and demonstrate technologies before moving to large-scale trials. A
143 solvent-based carbon capture plant is directly connected to PACT combustion facilities which
144 is capable of capturing one ton of CO₂ per day from an equivalent of approximately 150kW
145 conventional coal combustion flue gas.

146 A simplified flow diagram of the plant is shown in Figure 1. Specification of the pilot plant
147 used for these tests are given in Table 1. The plant has full absorption and desorption cycle and
148 is equipped with absorber, stripper, reboiler, cross exchanger, carbon filter and water wash. Its
149 gas pre-treatment section can be used either as Flue Gas Desulphurisation (FGD) or Direct
150 Contact Cooler (DCC). The plant has an activated carbon filter to remove some of the
151 degradation products from the solvent. Temperatures of flue gas and lean solvent entering the
152 absorber are controlled. The absorber has 6.5m structured Mellapak CC3 packing while stripper
153 is packed with 7.5m of IMTP25 random packing. Absorber and stripper temperature profile
154 along the height of the columns is measured by 8 and 5 RTDs, respectively. Gas analysis are
155 performed at 5 different locations in the plant. Sampling lines are located at the FGD inlet,
156 absorber inlet, water wash inlet and outlet, and stripper outlet. Gaset DX4000 FTIR is used
157 for gas analysis which sequentially detects samples from each of the locations. The sequence
158 and sampling time is user defined and can be changed in the FTIR software as and when
159 required. Stripping is performed in the reboiler supplied with pressurized hot water (PHW)
160 generated by electrical heating. The PHW has a bypass to control the flow rate through the
161 reboiler or bypassing it. A pneumatically driven 3-way valve is used for this purpose. The
162 energy used for stripping is calculated by measuring the flow rate, inlet and outlet temperatures
163 of the PHW. Stripper pressure is controlled automatically to a user defined set point. The plant
164 uses two different data logging systems. National Instruments PXi system is used to log most
165 of the data from the plant while Allen Bradley PLC is used to control the plant and log relevant
166 data.

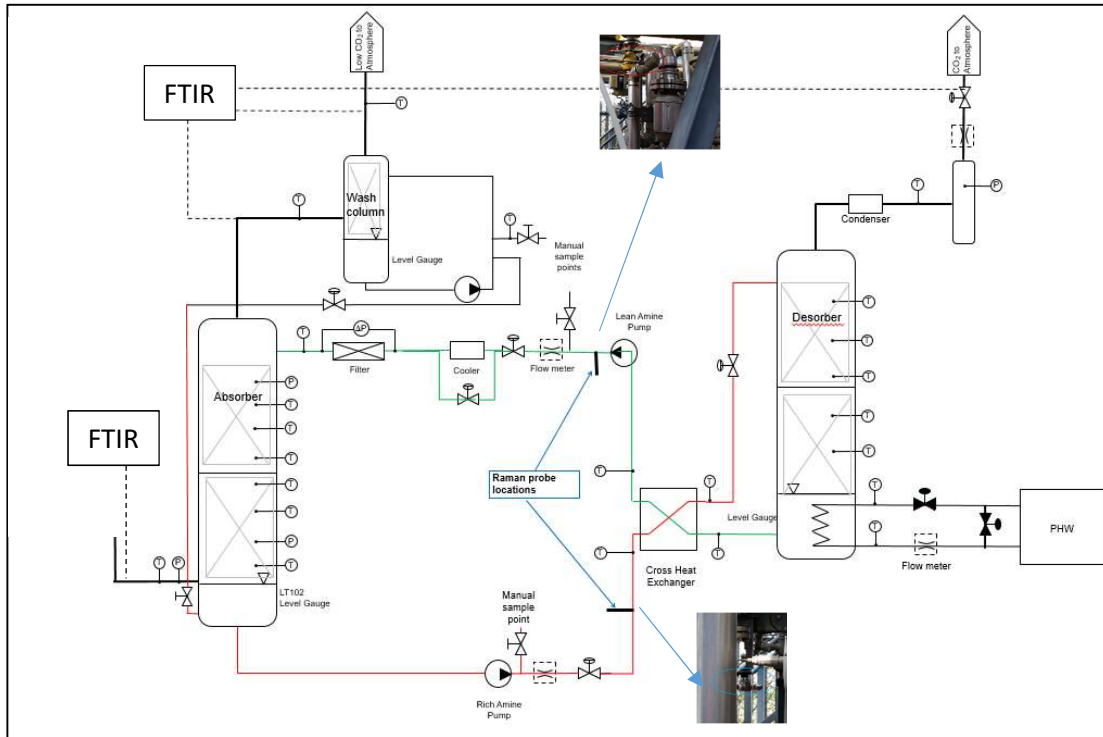
167 Table 1: Absorber and stripper specifications

Specifications	Absorber	Stripper	Water wash
Diameter (mm)	300	300	300
Packing name	Mellapak CC3	IMTP25	IMTP25
Packing type	Structured	Random	Random
Packing height (m)	6.5	7.5	7.5
Temperature measurements	10	9	-

168
169 The Raman spectra were obtained by Kaiser RXN2 multi-channel 785 nm spectrometer with
170 400mW maximum laser power. Two Raman immersion optic probes (1/4" diameter, 6" length,
171 short focused, sapphire window) were directly connected to lean and rich amine process lines
172 at PACT amine plant as shown in Figure 1. iC Raman 4.1 software was used to acquire Raman
173 signals maintaining approximately 1-minute interval during each measurement. Each spectra
174 were exported to Matlab 2017 for preprocessing. Locations of Raman measurements were
175 selected to reasonably represent lean and rich stream solvent concentrations. Distances from

176 the nearest manual sampling points to the lean and rich Raman probes were 120 cm and 106
177 cm respectively.

178



179

180

Figure 1: Simplified plant layout with raman probe locations

181 The accuracy of the real-time predictions were argued by comparing their values with offline
182 liquid sample analysis and their sensitivity to process conditions. Offline liquid analysis were
183 performed to determine CO₂ loading and amine concentration as described in Akram et al.
184 (2016). Mettler Toledo T90 auto-titrator was used to perform acid-base titration where HCl
185 (0.2M) was used to determine total amine concentration and NaOH (0.5M) was used to
186 determine CO₂ concentration. Uncertainties in the titration procedure were determined by
187 preparing a solution of MEA (nominal concentration 29.4%) and loading to 8.04% CO₂ by
188 weight gravimetrically by bubbling CO₂ through it. Three samples from MEA solution thus
189 prepared were then titrated using the titration apparatus to measure MEA concentration and
190 CO₂ loading. The average uncertainty in the loading measurements was found to be +/- 3.15%.
191 This procedure is similar to the previously reported method by Tait *et al.* (2018).

192 Gas composition was measured by two FTIR instruments, one was used to consistently measure
193 gas composition at the outlet of the absorber, while the other was used to measure gas
194 composition at the inlet of the absorber but was also used to measure at other plant locations
195 from time to time. The gas samples are extracted from the plant using isokinetic sampling
196 probes and routed to the FTIR through heated filters, heated sampling lines and heated cabinet
197 housing solenoid for sample switching. The entire sampling system was heated up to 180 °C to
198 avoid condensation.

199 For the first two test campaigns air with CO₂ injection was used as flue gas. During the last
200 test, flue gas from coal combustion was used. The coal flue gas was not passed through FGD
201 so had high concentrations of SO₂. Presence of SO₂ in the flue gas results in faster degradation

202 of solvent. The aim of this tests was to investigate if Raman Spectroscopy measurements are
 203 influenced by solvent degradation. The tests were performed with 30% MEA which had been
 204 used for 10 days with normal plant operation. The solvent was transparent in appearance by the
 205 time of first use.

206 2.2 Selection of process variable matrix

207 The tests were divided into three campaigns.

- 208 1. Absorption-desorption
- 209 2. Process variations
- 210 3. Coal flue gas

211 Details of the three test campaigns are given in the following sections.

212 2.2.1 Absorption-desorption:

213 The aim of the absorption-desorption test campaign was to check the accuracy of the predictions
 214 by Raman spectroscopy throughout a complete absorption and desorption cycle, and observing
 215 whether the two Raman sensors can generate identical results when measuring the same sample.
 216 The test was divided into two phases, absorption and desorption, so that during the absorption
 217 process there was no desorption and vice versa. The conditions for the test (Tests 1 & 2) are
 218 given below, in Table 2.

219 Table 2: Conditions for absorption-desorption test

Absorption			Desorption		
Test 1			Test 2		
Parameter	Value	Unit	Parameter	Value	Unit
Flue gas flow rate	210	m ³ /h	Flue gas flow rate	NA	m ³ /h
CO ₂ concentration	12	v/v%	CO ₂ concentration	NA	v/v %
Solvent flow rate	900	kg/h	Solvent flow rate	900	kg/h
Stripper pressure	NA	bar	Stripper pressure	0.6	bar
PHW set point	NA	°C	PHW set point	128	°C
PHW flow rate	NA	m ³ /h	PHW flow rate	9.8	m ³ /h

220

221 2.2.2 Process variations:

222 During these tests, the CO₂ capture plant was operated with full absorption and desorption cycle
 223 and the Raman spectroscopy predictions were monitored. Operational conditions, given in
 224 Table 3, were varied to investigate the response of Raman instruments against these variations.
 225 Solvent flow rate, gas flow rate and CO₂ concentrations were changed. The test was started
 226 with around 190 m³/h gas flow with 5% CO₂ concentration, 600 kg/h solvent flow (Test 3).
 227 CO₂ concentration was increased to 12% for the Test 4. Solvent flow rate was increased to 1000
 228 kg/h and 1200 kg/h for the Test 5 and Test 7, respectively. Flue gas flow rate was reduced to
 229 150 m³/h for the Test 6. Operational data was recorded throughout the test period and manual
 230 samples for rich and lean solvent were collected for bench analysis at 30 minute intervals during
 231 this test campaign.

232

233

Table 3: conditions for process conditions variation tests

Parameter	Value	Units	Parameter	Value	Units
Test 3			Test 4		
Flue gas flow rate	193	m ³ /h	Flue gas flow rate	193	m ³ /h
CO ₂ concentration	5	v/v %	CO ₂ concentration	12	v/v %
Solvent flow rate	600	kg/h	Solvent flow rate	600	kg/h
Stripper pressure	0.4	barg	Stripper pressure	0.4	barg
Test 5			Test 6		
Flue gas flow rate	193	m ³ /h	Flue gas flow rate	150	m ³ /h
CO ₂ concentration	12	v/v %	CO ₂ concentration	12	v/v %
Solvent flow rate	1000	kg/h	Solvent flow rate	1000	kg/h
Stripper pressure	0.4	barg	Stripper pressure	0.4	barg
Test 7					
Flue gas flow rate	150	m ³ /h	Solvent flow rate	1200	kg/h
CO ₂ concentration	12	v/v %	Stripper pressure	0.4	barg

234

235 2.2.3 Coal flue gas:

236 For the first two test campaigns air with CO₂ injection was used as flue gas. The main idea of
 237 this test was to investigate if the spectrometer can accurately predict CO₂ loadings if solvent is
 238 degraded by the presence of SO₂ in flue gas. For this purpose flue gas from a coal fired
 239 combustor was fed to the CO₂ capture plant absorber.

240 The flue gas was generated by burning bituminous El Cerrejon coal in the 250 kW PACT
 241 air/oxy-fired CTF (Combustion Test Facility), operated in air-firing mode. The furnace
 242 chamber is cylindrical in shape, 0.9 m in diameter and 4 m long, and it is fitted with a scaled
 243 version of a Doosan Babcock Mark III Low-NO_x burner in a down firing arrangement. The flue
 244 gas produced was passed through a cyclone and then a high temperature candle filter for
 245 particulate removal before a slip stream of it was introduced into the CO₂ capture plant.

246 The capture plant has a gas pretreatment section which can be employed as FGD for removing
 247 Sulphur but for these tests FGD was deliberately not operated in order to send SO₂ to the capture
 248 section to accelerate solvent degradation. Carbon filter was also totally bypassed during this
 249 test campaign for the same reason. The average concentration of SO₂ in the flue gas entering
 250 the absorber was around 210ppm. However, due to short duration of the test, a considerable
 251 colour change in the liquid samples, which is an indication of solvent degradation, could not be
 252 observed. Conditions for the test are given in Table 4. The following measures were adopted to
 253 accelerate solvent degradation.

- 254 • Flue gas with 210ppm of SO₂ was fed into the absorber
- 255 • Lean solvent temperature was increased to 55 °C
- 256 • Stripper pressure was increased to 0.6 barg to heat up the solvent to a higher temperature
- 257 • PHW set point temperature increased to 133 °C

258 Due to a plant trip and some sump level instability in the absorber sump, the PHW temperature
 259 set point, lean solvent temperature set point and stripper pressure set point were adjusted to 128
 260 °C, 50 °C and 0.4 barg, respectively.

261

262 Table 4: Test conditions for coal flue gas

Parameter	Value	Units	Parameter	Value	Units
Test 8			Test 9		
Flue gas flow rate	200	m ³ /h	Flue gas flow rate	200	m ³ /h
CO ₂ concentration	12.7	v/v %	CO ₂ concentration	12.7	v/v %
SO ₂ concentration	210	ppm	SO ₂ concentration	210	ppm
Solvent flow rate	1000	kg/h	Solvent flow rate	1000	kg/h
Stripper pressure	0.4	barg	Stripper pressure	0.6	barg
Lean solvent temperature	40	°C	Lean solvent temperature	55	°C
PHW set point	128	°C	PHW set point	133	°C
Test 10					
Flue gas flow rate	200	m ³ /h	Solvent flow rate	1000	kg/h
CO ₂ concentration	12.7	%	Stripper pressure	0.4	barg
SO ₂ concentration	210	ppm	Lean solvent temperature	50	°C
PHW set point	128	°C			

263

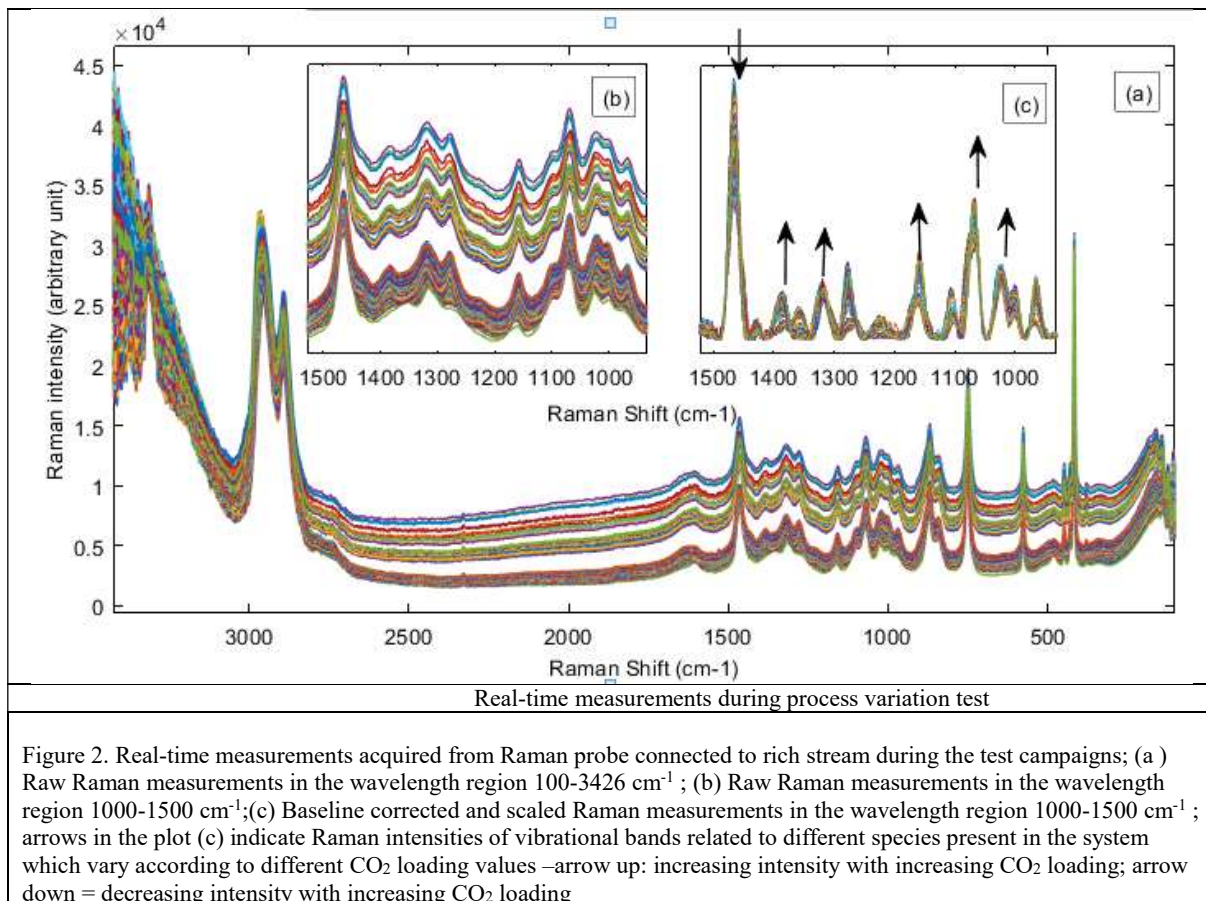
264 **3. Results and Discussion**

265 The results of the three test campaigns are presented in four sections. In section 3.1, real-time
 266 Raman predictions are compared with titration measurements. The next three sections discuss
 267 the plant trends and how effectively the real-time monitoring tool can correlate to the plant
 268 performance during the three test campaigns.

269 3.1. Raman model predictions with titration measurements

270 The reaction between CO₂ and MEA is complex and there is still a controversy regarding it's
 271 detailed understanding (Xie *et al.*, 2010). However, in Raman spectroscopic point of view, it
 272 should be possible to identify the fate of reactants and products according to the behavior of
 273 peaks corresponding to Raman active vibrational modes. The reactant-product pool of MEA-
 274 CO₂-H₂O system contain carbon ion species as carbonate, bicarbonate, carbamate and amine
 275 species as protonated amine and unreacted amine. These chemical species show their
 276 identification in different wavelength areas of a Raman spectrum (Jinadasa *et al.*, 2017). The
 277 region from 767-1525 cm⁻¹ was used to determine the CO₂ loading for the study because this
 278 region is rich with vibrational modes related to carbon species. Figure 2 shows Raman spectra
 279 obtained during the test with process variations. The raw Raman measurements (Figures 2a, 2b)
 280 show different baseline drifts but once they are baseline corrected and scaled, their spectral
 281 variations in the fingerprint region become easy to identify the chemical components as can be
 282 seen in Figure 2c. The upward arrows in Figure 2 indicate the chemical species (carbonate,
 283 bicarbonate, carbamate and protonated amine) as their concentrations increase with increasing
 284 CO₂ loading, while the downward arrows point to a vibrational band of free MEA which yields
 285 lower concentration as the CO₂ loading is increasing.

286 The fingerprint area of baseline corrected Raman spectra was used to determine CO₂ loading
 287 after applying multivariate calibration approach. The initial regression model development can
 288 be found in (Jinadasa, 2019) and the path of how it modified to the PACT plant operation is
 289 described in the second part of this paper.



290

291 3.2 Campaign 1 – Absorption and desorption

292 The campaign was divided into two separate tests, one each for absorption and desorption. This
 293 section presents results of the absorption and desorption tests, separately. In order to avoid
 294 confusion, it is essential to clarify here that rich loading refers to the measurement at the outlet
 295 of the absorber and lean loading refers to the measurement at the outlet of the reboiler,
 296 regardless of whether the absorption/desorption process was in operation or not.

297 Please note that for these tests steady state conditions were not achieved as there was no
 298 stripping during absorption and vice versa. Steady state is normally defined by the steady CO_2
 299 concentrations at the absorber outlet. However, it was not possible to achieve this condition
 300 during these tests.

301 3.2.1. Absorption:

302 Conditions for this test were, 900 kg/h solvent flow and 210 m^3/h flue gas with 12% CO_2 . To
 303 calculate real time CO_2 capture efficiency, two FTIR instruments, at the inlet and outlet of the
 304 absorber, were used to measure CO_2 concentration in the flue gas. The plant was operated in
 305 absorption mode until the CO_2 concentration in the flue gas leaving the absorber was almost
 306 equal to that entering the absorber, which indicated that the solvent was approaching its
 307 maximum CO_2 loading under the conditions of the test.

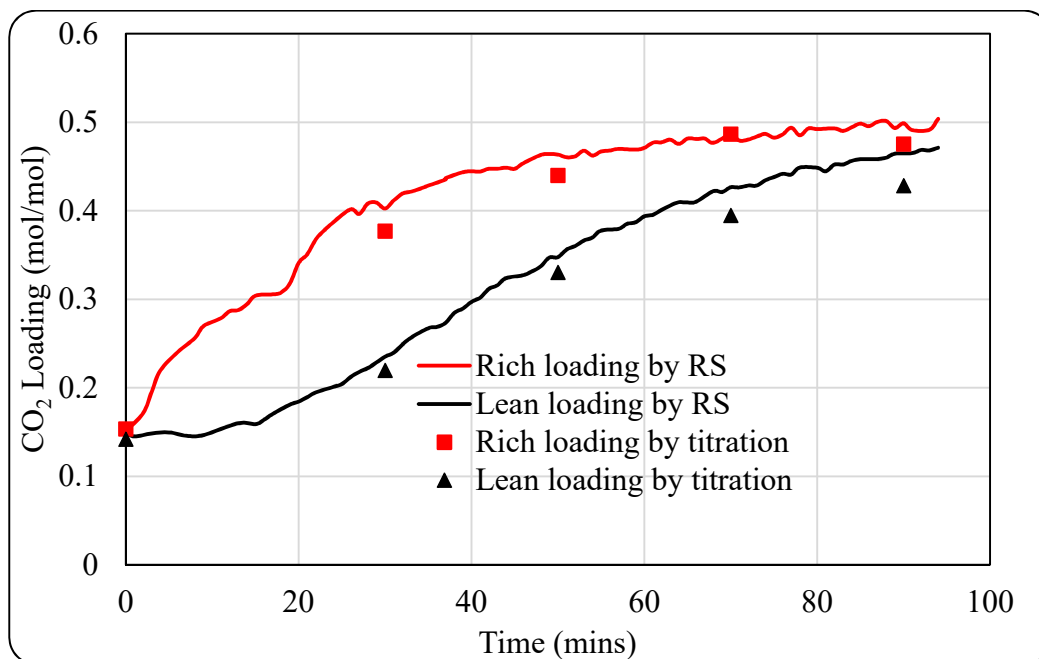
308 During absorption, there was no supply of PHW to the reboiler so the absorber was the only
 309 location where process changes happened. Theoretically, under this scenario, rich solvent
 310 coming out from the absorber bottom should have the same CO_2 loading as that leaving from

311 the bottom of the desorber/reboiler. However, in reality, due to the plant configuration this was
312 not the case. The reboiler is a shell and tube heat exchanger, having solvent on the shell side,
313 which contains most of the solvent inventory, around 90%, of the plant. Rich solvent coming
314 from the absorber mixes with the solvent already in the reboiler and gets diluted so the loading
315 in both the rich and lean is expected to be different depending upon the operational conditions.

316 Rich and lean solvent loadings as measured by Raman probes and titrations are presented in
317 Figure 3. Solid lines are representing continuous measurement by Raman Spectroscopy while
318 point values are representing titration data. Due to the close proximity of manual sampling
319 points and Raman probes, circulation times between them for both the rich and lean solvent
320 streams were less than 5 seconds for all the flow conditions tested. In an ideal situation, for
321 comparison, manual samples should be taken at the exact same time as the Raman sensor
322 updates its output, but it is not possible to time it exactly.

323 As the solvent was used in previous tests, it had some unstripped CO₂ in it so these tests were
324 started with a lean solvent. After starting solvent circulation, samples were taken for titration
325 from both lean and rich solvent streams before the introduction of flue gas. These measurements
326 indicated that, before starting the test, the lean and rich solvent streams had CO₂ loading of
327 0.1419 mol/mol and 0.1534 mol/mol. After starting solvent circulation, synthetic flue gas was
328 introduced to the absorber, causing the rich solvent loading to increase. This highly loaded
329 solvent then mixed with the lean solvent in the reboiler sump. Therefore, lean loading is always
330 lower than the rich loading, also increment in lean loading is more gradual while that in rich
331 loading is relatively sharper, see Figure 3.

332



333

334 Figure 3: Comparison of CO₂ loadings measured by Raman spectrometer and titrations

335 Figure 3 shows that there is a good agreement between titration data and the Raman predicted
336 values in the whole operation range. During the absorption cycle, the average Raman prediction
337 error was reported as +/-0.009 mol/mol loading by the multivariate model. This concludes that

338 through the Raman prediction curves, it is now possible to discuss and comment on the
339 absorption performance under various process conditions.

340 As soon as the flue gas was introduced to the absorber, the rich Raman measurement showed
341 an increment in the CO₂ loading while the lean Raman measurement took some time to show
342 the same concentration due to the reasons explained above. Lean loading reached a value of
343 0.44 mol/mol after around 37 minutes of rich loading. These findings are similar to those
344 demonstrated in Tait et al. (2018) where time to fully mix the contents of the absorber and
345 reboiler for this plant was found to be 37-38 minutes using conductivity probes, one each at the
346 inlet and outlet of the absorber and stripper. This test also proves that the Raman spectroscopy
347 can be used to determine the solvent circulation times inside the plant.

348 Absorber temperature profile:

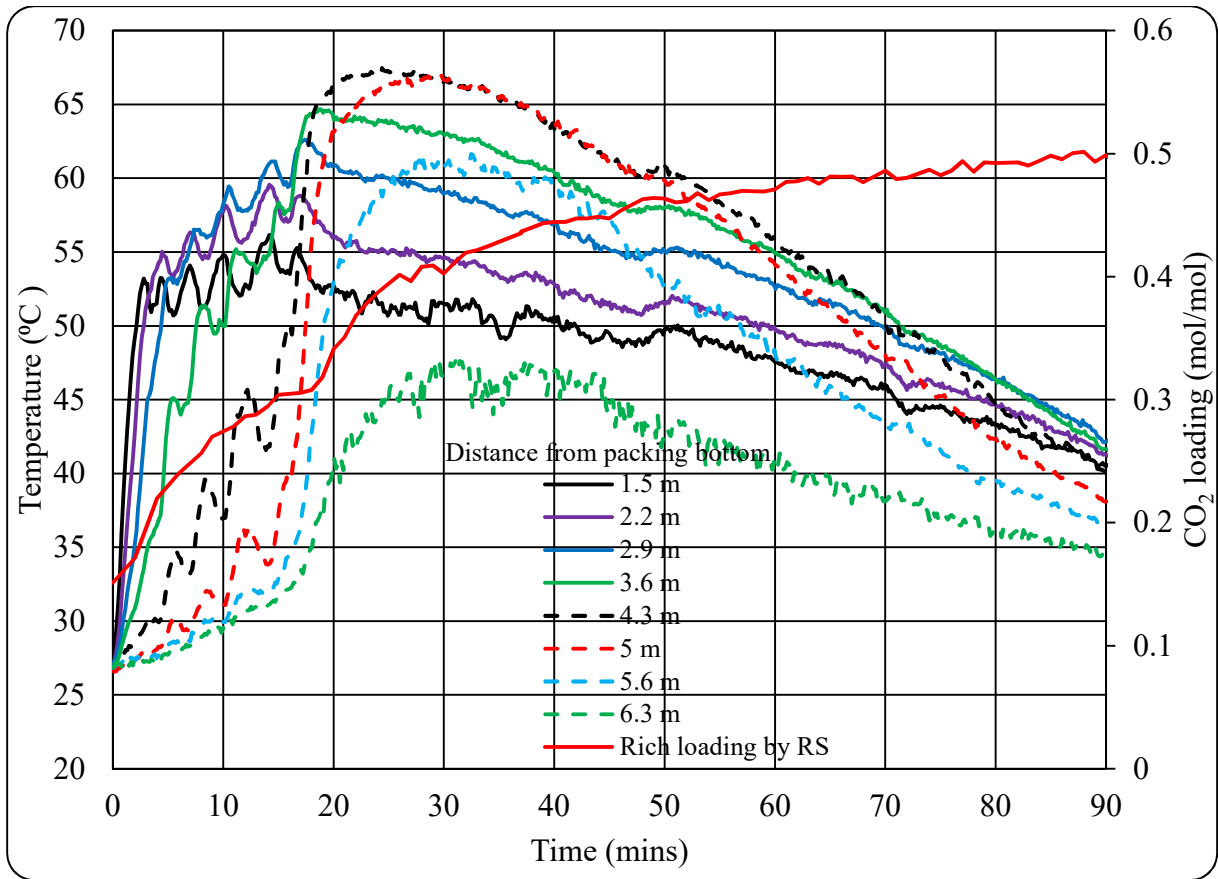
349 Figure 4 plots the temperature profile inside the absorber. The temperatures are plotted against
350 time for different locations along the height of the absorber starting from the bottom of the
351 packing. When flue gas is initially fed to the absorber, temperatures at the bottom of the
352 absorber increased sharply in comparison to those further up in the column. This implies that
353 lean solvent first comes in contact with the flue gas at the bottom. However, after some time,
354 temperatures in the middle of the column increased sharply as compared to those at the bottom
355 and top. Moreover, the temperature bulge is observed at 2/3rd of the packing height, indicating
356 the maximum reaction point. These observations coincide with rich CO₂ loading measurements
357 by Raman Spectroscopy, plotted on the same graph. The Raman predictions of the CO₂ loading
358 in the rich amine stream is increased drastically until the temperature profile inside the absorber
359 reaches its maximum. The temperatures started to decrease as the gradient of the increment in
360 CO₂ loading in the rich amine stream was decreased. This is due to the temperature dependency
361 and exothermic nature of the CO₂ absorption process. As the difference between the lean and
362 rich loading is decreased, proportionally the temperatures inside the absorber also drop. This
363 absorption test confirms that both Raman probes measurements in lean and rich streams were
364 able to follow the absorption phenomenon.

365 Capture efficiency:

366 Concentration of CO₂ in the inlet gas was fixed at 12%. Concentration of CO₂ in absorber exit
367 gas increased gradually from below 1% to close to 12%. Figure 5 plots CO₂ capture efficiency
368 against time during the absorption process. As can be witnessed from the plot, at the start of the
369 test, capture efficiency was around 97% and it remained almost steady for about 14 minutes, at
370 which point it dropped sharply and steadily to below 20% within one hour. As solvent was not
371 being stripped, its loading capacity gradually reduced and reached a point where there was no
372 further absorption i.e. concentration of CO₂ in the gas leaving the absorber was approximately
373 the same as that entering the absorber.

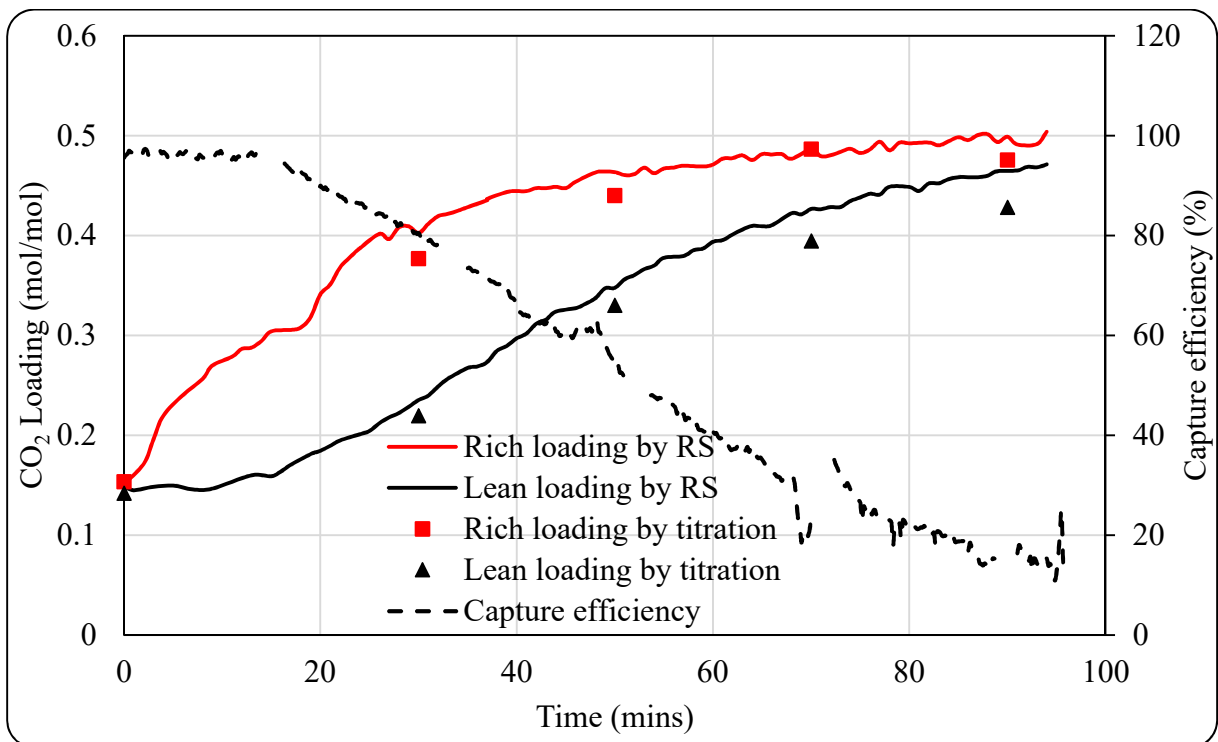
374

375



376

377 Figure 4: Absorber temperature profile during absorption cycle (Temperature measurements
378 locations are measured from the bottom of packing)



379

380

Figure 5: Capture efficiency change with time during absorption

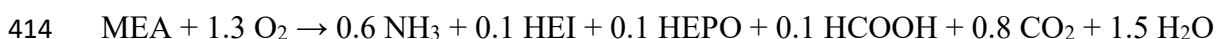
381 The Raman measurements plotted on the same graph also show the same trends. At the
382 beginning both of the loadings were almost the same. Then, rich loading started to increase
383 sharply as flue gas was introduced. Lean loadings started to increase with some delay caused
384 by the solvent inventory in the reboiler sump. Raman measurements indicate that difference
385 between rich and lean loadings was quite high for around 45mins of the test period and then
386 started dropping as capture efficiency reached below 55%. Towards the end of the absorption
387 test, both of the loadings again become closer to each other towards the rich loading limit of
388 the solvent.

389 As CO₂ injection rate is controlled separately and is not directly linked to concentration of CO₂
390 in the flue gas, at around 70 minutes, CO₂ concentration dropped to 11% due to some process
391 issues. Due to this reason the capture efficiency plot shows an increase at this time.

392 Emissions:

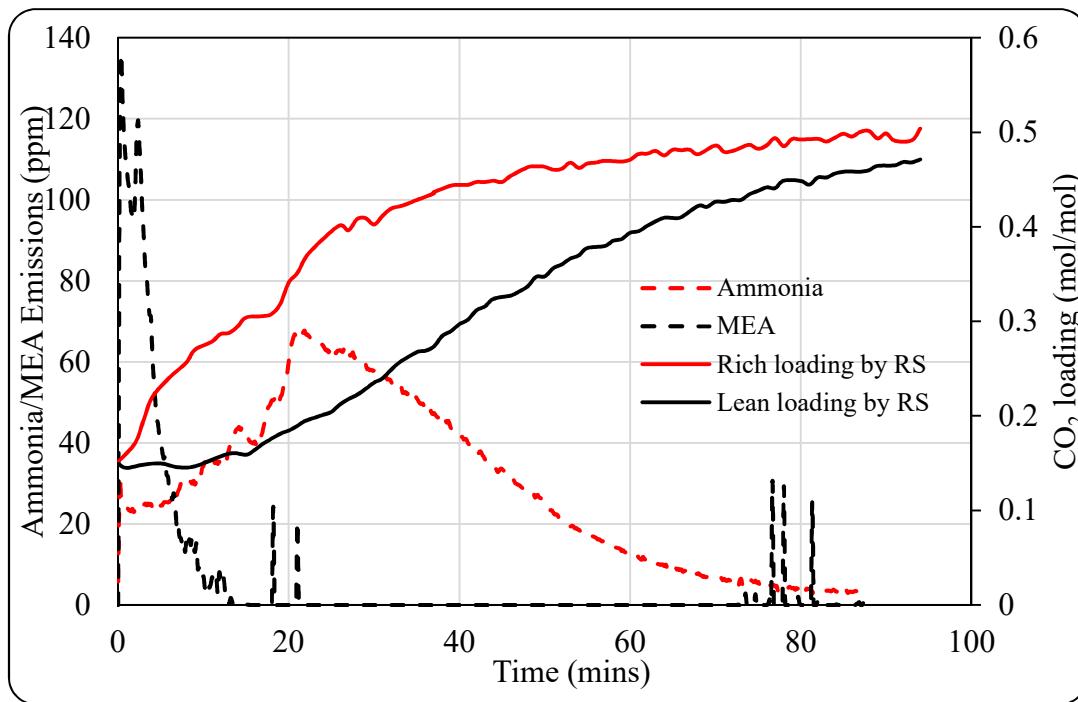
393 Figure 6 shows emissions of MEA and ammonia during the absorption process. MEA emissions
394 were observed to be very high at the start, then reduced to almost zero after 13 minutes and
395 remained low throughout the test. The initial high level of MEA was thought to be due to the
396 start of the process. At the start solvent is very lean and reaction rate between MEA and CO₂ is
397 relatively higher. Higher rate of reaction can result in higher rate of degradation and thus can
398 be the cause of higher MEA evaporation from the absorber. However, most of the MEA carried
399 over with the flue gas from the absorber was removed by water wash. The FTIR instrument is
400 installed on upright pipe so there is a U-bend just before the measurement. The carried over
401 water and solvent from the absorber tend to condensate and accumulate in the U-bend. A drain
402 is provided at this point which feeds condensate back to the absorber. However, sometimes the
403 U-bend does not drain fully and result in flash of the condensate into the sampling point filter
404 resulting in increased MEA point measurements. The occasional peaks of 20-30 ppm of MEA
405 observed in Figure 7 are due to this phenomenon.

406 Degradation of MEA during the cyclic operation is a significant problem. Knudsen et al. have
407 reported a loss of MEA of 2.4 kg per ton of CO₂ captured [Knudsen et al. 2007]. The
408 degradation can happen by two mechanisms. Thermal degradation occurs at stripper conditions,
409 high temperature and abundance of CO₂ [Rochelle, 2012, Kohl and Nielsen, 1997]. Oxidative
410 degradation occurs at lower temperature and in the presence of oxygen. These conditions are
411 available in the absorber. It is thought that oxidative degradation is dominant degradation
412 pathway for MEA [Da Silva et al. 2012, Lepaumier et al. 2011]. Leonard et al. [26] proposed
413 a model for oxidative degradation described the following over all reaction.

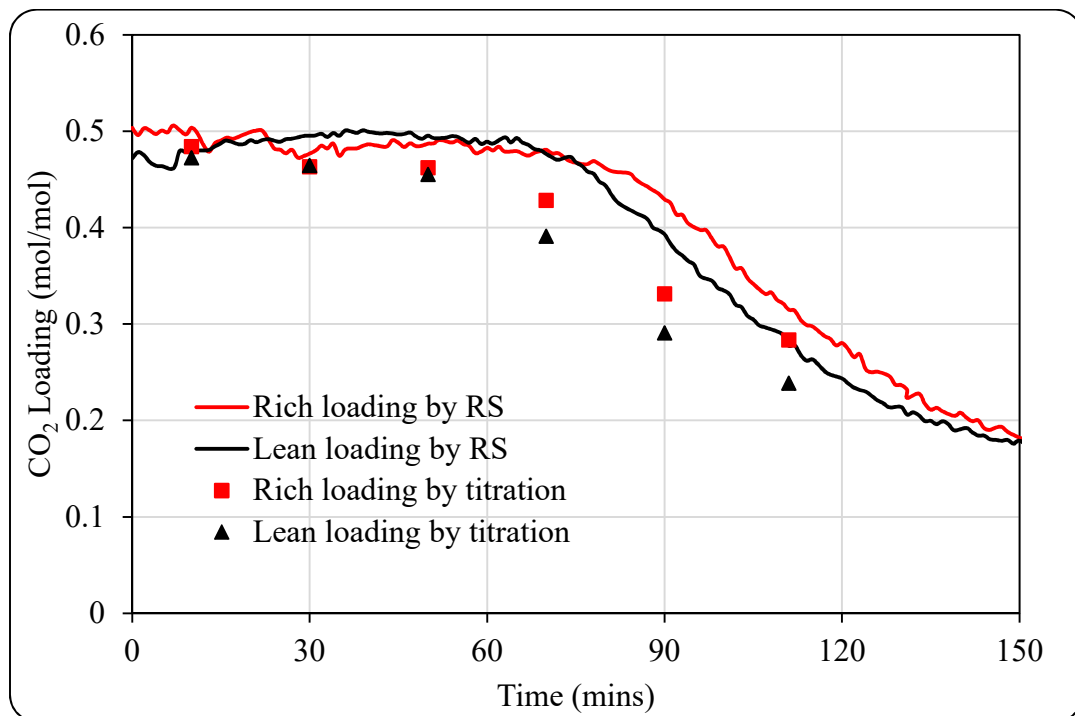


415 The reaction indicates that Ammonia is the main degradation product which exits with the flue
416 gas. It is essential to monitor the emissions of ammonia during the process to assess
417 environmental burden of the process. Ammonia emissions started at a value of around 30ppm
418 and peaked at 67ppm. After this the emissions started decreasing and become very low to a
419 value of below 10ppm. The emissions seem to follow the absorption phenomenon as can be
420 observed from rich and lean loadings as measured by Raman probes. Ammonia emissions
421 increase at the start due to increase in loading due to absorption of CO₂, reaches a peak value
422 and then start decreasing due to drop in reaction rate. The similar phenomenon is followed by

423 Raman measurements indicating that Raman Spectroscopy can be employed to monitor process
 424 variations in CO₂ capture plants.
 425



426
 427 Figure 6: Emissions of MEA and Ammonia (NH₃) during absorption process



428
 429 Figure 7: Comparison of CO₂ loadings during desorption measured by Raman spectrometer
 430 and titrations
 431

432 3.2.2. Desorption

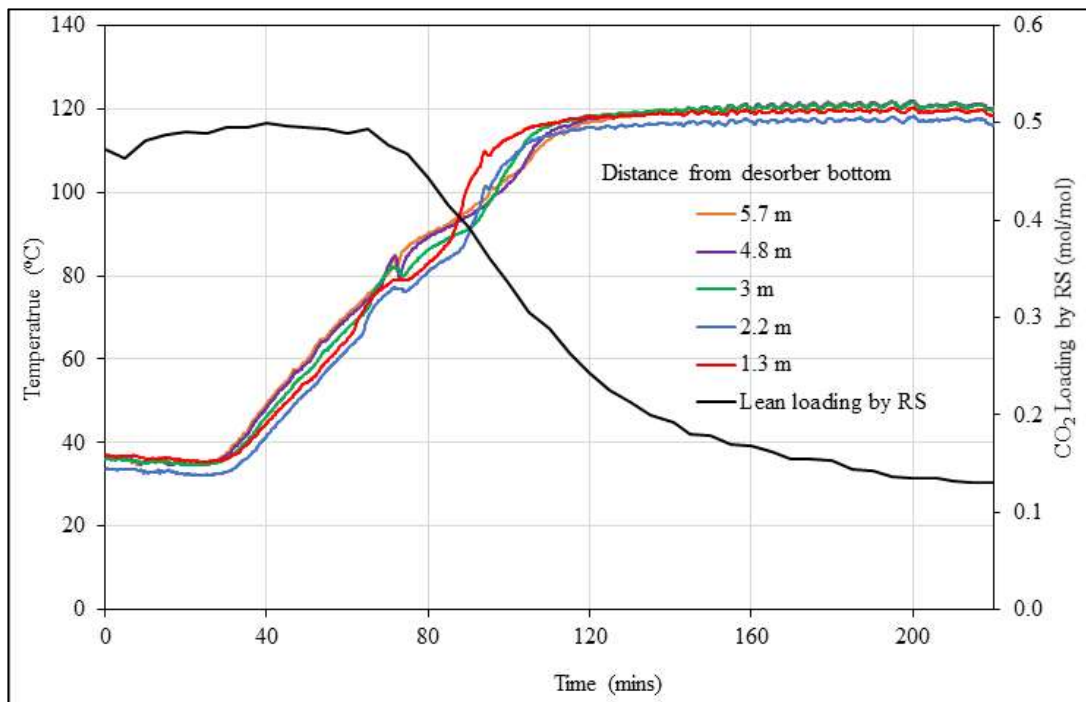
433 After completion of the absorption cycle, flue gas was turned off and desorption cycle was
434 started by supplying pressurized hot water to the reboiler. The aim of this desorption cycle test
435 is to monitor the predictive capacity of Raman instrument during a complete desorption cycle
436 in which CO₂ is stripped from saturated solvent. Figure 7 shows the comparison of Raman
437 predictions in rich and lean solvent streams with respect to the titration measurements. Both
438 rich and lean loadings start dropping after some time of starting the desorption cycle. The delay
439 was due to the time taken for the solvent to heat up. Both of the loadings drop due to CO₂ being
440 stripped from the solvent but no absorption due to stoppage of flue gas to the absorber. Both
441 the rich and lean Raman measurements are high than the titration data. This may be due to the
442 same model being used to predict both of the data sets.

443 Similar to the absorption cycle, during the entire desorption phase, the inline Raman predictions
444 show good agreement with the offline measurements by conventional titration methods.
445 However, during desorption cycle rich and lean loadings are closer to each other as compared
446 to absorption cycle. This is due to less solvent inventory in the absorber, only 10% of the total
447 plant inventory. Lean solvent from desorber mixes with the solvent in the absorber sump and
448 thus loading changes.

449 Temperature distribution in the stripper:

450 The stripper temperature profile is plotted against time alongside CO₂ loading measurements
451 by Raman probes, in Figure 8. The Fig shows that temperatures throughout the stripper column
452 are identical throughout the test. The temperatures increase linearly at the start of the PHW
453 supply until reaching a peak value before becoming steady. Total time for stripping was
454 calculated to be 3:20 hrs. The figure also shows that Raman measurements follow the
455 desorption process. Plot indicates that both rich and lean Raman measurements became closer
456 after stopping absorption due to continued circulation as stripping was not started for a while
457 even after PHW flow was started. Both the rich and lean loadings started dropping as the solvent
458 heated up to the stripping temperature. The stripping rate was very high as column temperatures
459 increase above 80 °C. This is marked by a rapid drop in both rich and lean loadings for around
460 1.5 hrs, after which the stripping rate dropped and loadings did not change as much. Both of
461 the Raman probes followed the same trend with rich probe measurements are little higher than
462 the lean ones due to mixing with rich solvent in the absorber sump. The stripping process was
463 stopped by ceasing PHW supply to the reboiler when Raman measurements dropped to around
464 0.15 as it is not worth striping to lower loadings as it can result in dramatic increase in reboiler
465 duty.

466



467

468

Figure 8: Stripper temperature profile during desorption process

469

Emissions:

470

During the desorption cycle the stripper outlet CO₂ stream was monitored via FTIR analyzer. Concentration of MEA in the CO₂ stream is plotted against time in Figure 9. After 43 mins of opening the pressure control valve MEA emissions reached a peak value of 55 ppm and then started dropping.

473

474

Similar phenomenon was observed during absorption, where MEA emissions were higher at the start, then dropped as the process progressed indicating that solvent emissions are higher at the start of the process and then decrease as the process moves towards steady state. In the case of desorption, pressure control valve stays closed until pressure is built up to the set point. In Figure 9 for example the valve started opening at 65 mins. Up to this point any condensation of MEA is accumulated behind the control valve. The accumulated MEA leaves with the product gas when the pressure control valve opens. This is the reason the MEA emissions increased first then dropped to around 10 ppm. A steady test on this plant usually takes around 3-5 hrs depending upon the parametric changes. MEA emissions with the product gas during this period under the test conditions are estimated to be around 2 g.

483

484

Raman measurements for lean loading are also plotted in Fig 9. The plot indicates that MEA emissions start to increase as stripping process started as indicated by drop in loadings measured by Raman probes. Emissions started to drop as stripping process became slower and loadings dropped to lower values.

487

488

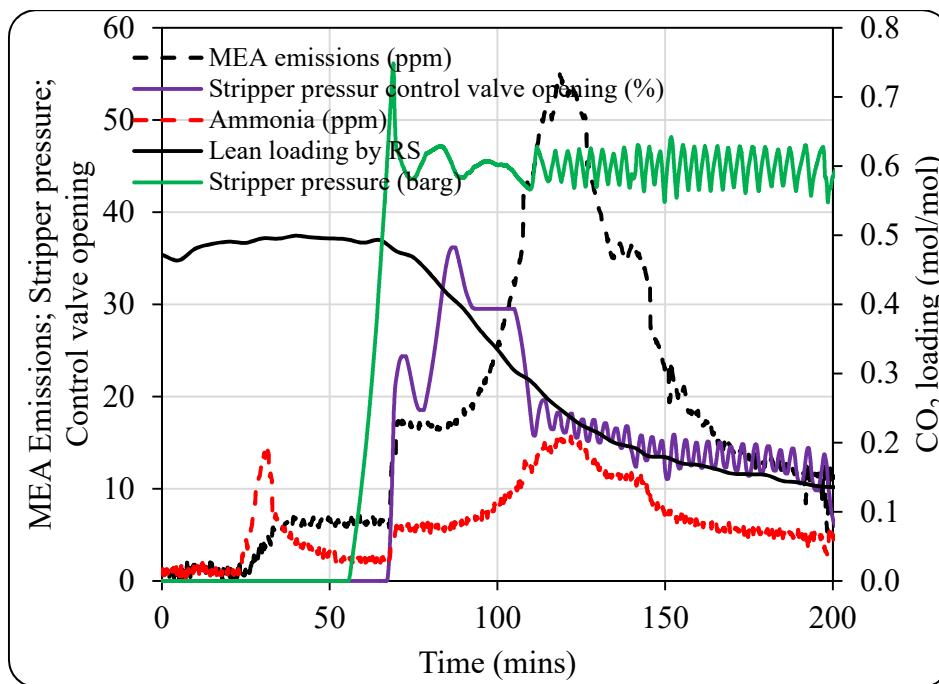


Figure 9: MEA emissions during stripping process

489

490

491 3.3 Tests with process conditions variations

492 During these tests, process conditions were varied. The test was started with 600 kg/h solvent
 493 flow and 193 m³/h gas flow with 5% CO₂ concentration (Test 3). The process parameters varied
 494 during the trial were increase/decrease in flue gas flowrate, CO₂ content (%vol) of the flue gas
 495 and solvent flow rate. Figure 10 shows the comparison of the rich and lean Raman
 496 measurements with the manual titration values. The rich and lean loadings first increase and
 497 then decrease without any process changes. This is due the fact that when the flue gas feed is
 498 started, solvent is lean. After the flue gas start up solvent starts absorbing CO₂, loadings start to
 499 increase but after some time when the solvent in the stripper is hot enough for stripping, the
 500 loadings start to drop.

501 The rich loading reached a maximum value of 0.44 mol/mol after CO₂ concentration was
 502 changed from 5% to 12%, (Test 4) while the lean loading remained between 0.108 mol/mol and
 503 0.229mol/mol during the entire test campaign. The figure shows that rich Raman measurements
 504 have better fit with the titration data as compared to lean Raman measurements.

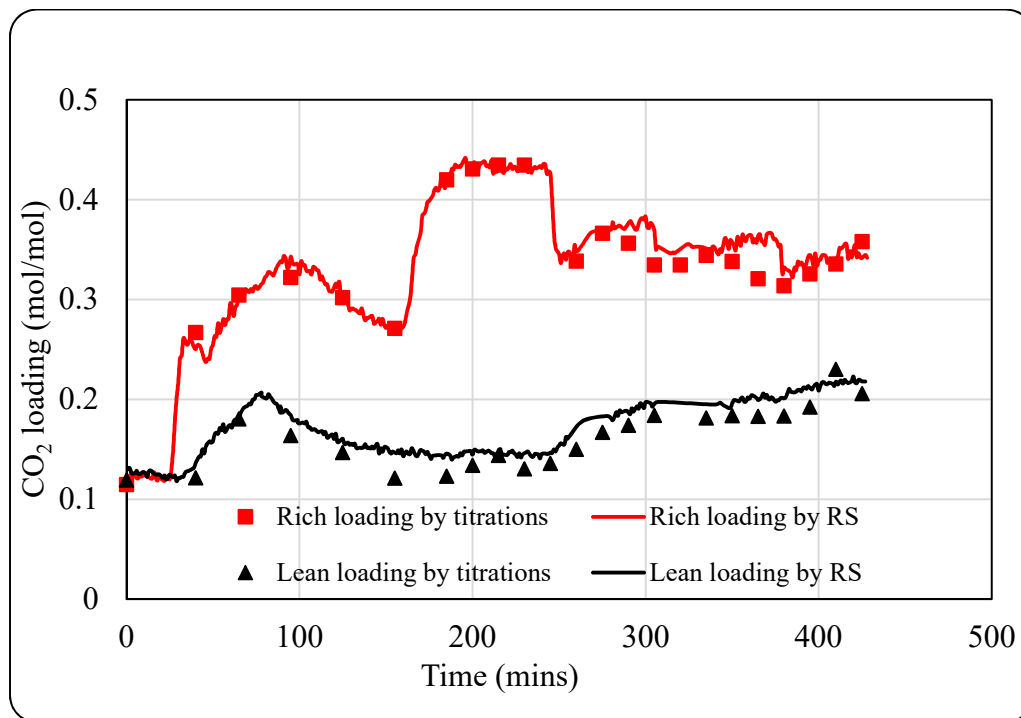
505 The impact of step changes in these parameters is more significant on the rich loading than that
 506 on the lean loading. The impact of process variations on the lean loading is delayed and
 507 dampened by dilution and mixing effects due to high solvent inventory in the reboiler.
 508 Therefore, it takes some time for the process changes effecting the rich solvent to be reflected
 509 in the lean solvent.

510 In the lean stream, the deviation of Raman measurements with respect to the titration results is
 511 higher as compared to that in the rich stream. This could be, due to the noise from new
 512 immersion probe and the new fibre optic cable connected to the lean stream. The multivariate
 513 model used in this study was developed from calibration and validation using the same
 514 immersion optic probe and fibre optic cable which were connected to the rich stream.
 515 Therefore, the instrument related noise from rich measurements are already accounted for in

516 the calibration model, whereas those from lean measurements are not encompassed. The
 517 deviation between the lean Raman measurements and lean titration values can be reduced by
 518 updating the existing calibration model by including new calibration samples from this PACT
 519 test campaign (Jinadasa, 2019).

520 Figure 11 plots process variations alongside loadings data. The plot shows changes in CO₂
 521 loadings as measured by Raman probes with respect to change in CO₂ concentration in the flue
 522 gas. As the CO₂ concentration was changed from 5 to 12%, rich loading increased rapidly from
 523 around 0.26 to 0.44 mol/mol. Lean loading increased steadily following a delay due to
 524 circulation times and mixing in the reboiler tank.

525



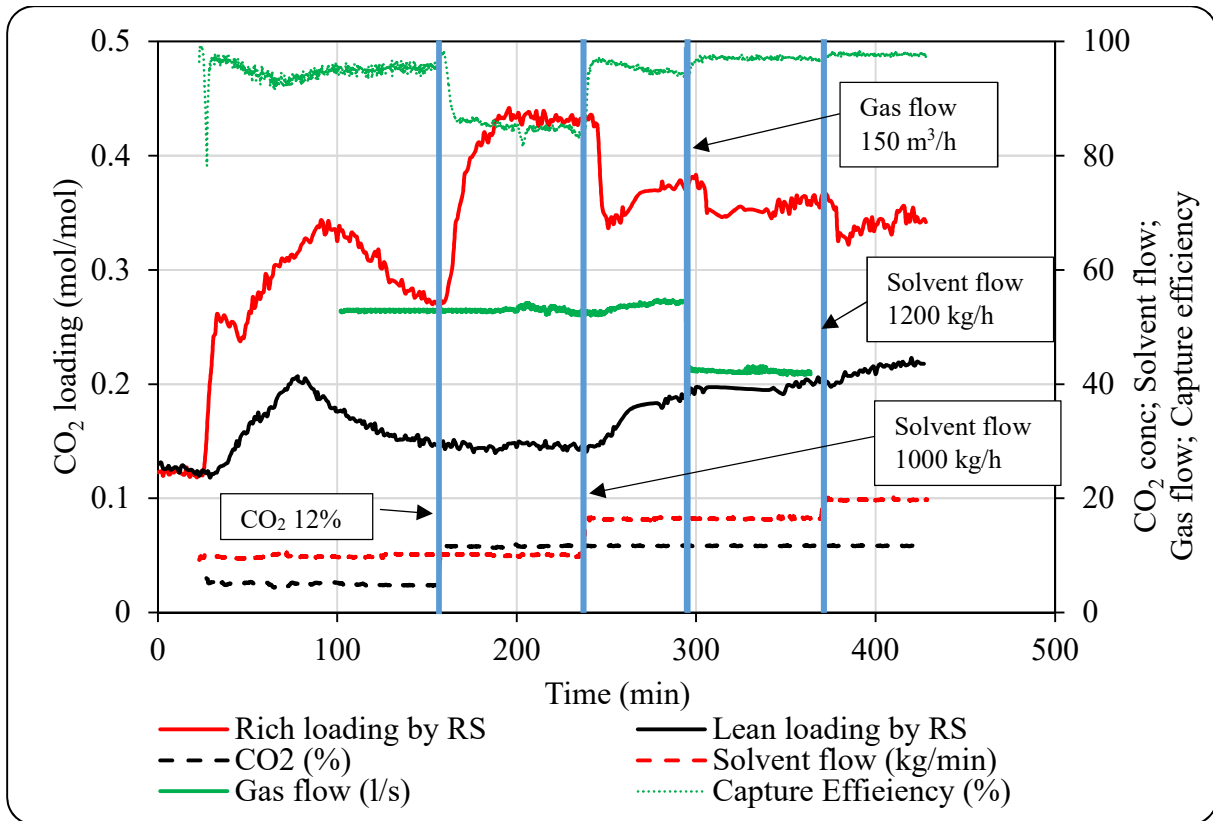
526

527 Figure 10: Comparison of Raman measurements and titration results for process variations

528

529 Figure 11 also plots solvent flow rate variations alongside Raman measurements against time.
 530 The tests were started at 600kg/h solvent flow rate, which was changed to 1000 kg/h and 1200
 531 kg/h during the course of the tests. As the solvent flow was increased from 600 to 1000 kg/h,
 532 Raman probe shown a sharp drop in rich loading, from 0.42 mol/mol to 0.33 mol/mol, then
 533 started increasing slowly. Lean loading measured by lean Raman probe also shown a slight drop
 534 and then started increasing slowly, lean amine loading increased from 0.148 to 0.179 mol/mol
 535 as the solvent flow rate was increased. As a result of increase in solvent flow rate, residence
 536 time in the reboiler decreased, resulting in drop in degree of stripping as the PHW supply
 537 conditions to the stripper remained the same. Due to increase in lean loading, rich loading also
 538 started increasing as absorber was receiving solvent with relatively higher lean loading.

539



540

541

Figure 11: Change in rich and lean loading with parametric variations

542

A similar phenomenon was observed when solvent flow rate was further increased to 1200kg/h. The rich Raman probe shown a drop in rich loading while lean Raman probe indicated a gradual increase in lean loading.

543

544

Figure 11 also plots variation in flue gas flow rate alongside Raman measurements against time. When flue gas flow rate was dropped from 190 m³/h to 150 m³/h, drop in rich loading was recorded by rich Raman probe. Lean Raman probe also shown a drop in lean loading at this point because solvent entering into the stripper was less loaded and due to stripper conditions unchanged, solvent leaving the stripper was also less loaded, although not proportionately.

545

546

547

548

549

550

Results indicate that even though there were several different process changes happening over a relatively short period of time, the Raman prediction model managed to observe the small changes in solvent loading and agreed well with titration results.

551

552

553

Capture efficiency: Capture efficiency is also plotted, against time, in Figure 11 alongside rich loading as measured by Raman probe. It can be seen from the plot that the capture efficiency was relatively higher, averaging around 95%, when 5% CO₂ concentration flue gas fed into the absorber. When the CO₂ concentration was increased to 12%, capture efficiency dropped to around 85%. During this test rich Raman measurements recorded a considerable increase while capture efficiency dropped indicating that the solvent did not have much capacity left in it to absorb a step in change in CO₂ concentration from 5% to 12%. Therefore, solvent flow was increased in the following test to increase solvent capacity. In this case, capture efficiency increased back to above 95% and rich loading dropped. Similar phenomenon can be observed for tests 6 and 7, where flue gas flow was decreased to 150 m³/h and solvent flow rate was increased to 1200

554

555

556

557

558

559

560

561

562

563

564 kg/h, respectively. In both cases capture efficiency increased but rich loading decreased due to
565 increase in solvent capacity as result of increase in L/G ratio.

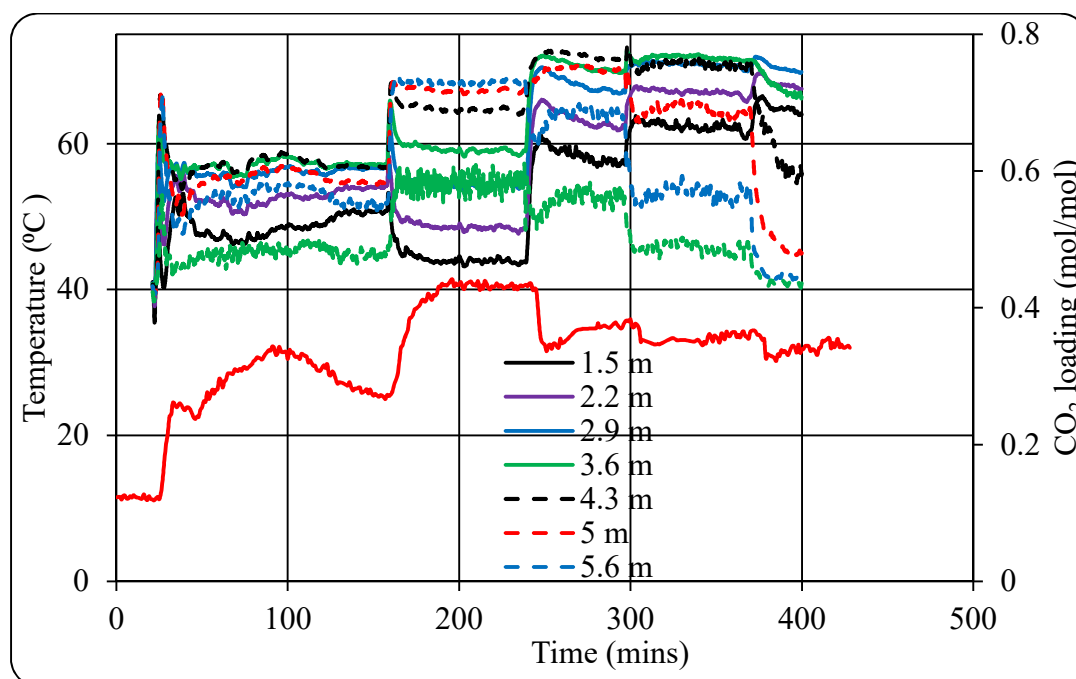
566 Absorber temperature profile:

567 Absorber temperature profile is plotted against time along the absorber height from the bottom
568 of the packing alongside Raman measurements in Figure 12. The temperature profiles at
569 different times indicate the effect of changes in operational parameters on the profile. It can
570 also be noted that the temperature profiles vary proportionally to the Raman measurements for
571 rich CO₂ loadings. The location of the peak (bulge) temperature in the absorber, varied with
572 variations in process parameters.

573 At low CO₂ concentration of 5% v/v (Test 3), the highest temperature (57 °C) was recorded just
574 above the middle of the column, between 3.6m and 4.3m from the bottom of the packing. The
575 top temperature measurement shown the lowest reading during this test due to most of the
576 reaction happening in lower part of the column and relatively cold lean solvent entering from
577 the top.

578 As the CO₂ concentration was increased from 5% to 12% (Test 4), bottom two temperature
579 measurements recorded a drop in temperature while rest of the six measurements recorded an
580 increase. The bulge temperature increased by 11 °C to 68 °C as the concentration was increased
581 to 12%. However, temperature at the bottom (1.5m) of the column dropped. Capture efficiency
582 dropped from above 95% for Test 3 to around 85% for this test due to the reason that solvent
583 flow rate is too low to absorb any more CO₂.

584



585

586 Figure 12: Changes in absorber temperature profile and Raman measurements with variations
587 in operational parameter

588 It can be witnessed from the plot that rich Raman probe recorded a sharp increase in rich loading
589 at this point which indicated that the Raman measurements followed the process. The bulge

590 also shifted up in the column, between 5m and 5.6m, as the CO₂ concentration was increased
591 to 12%. However, in this case the lowest temperature was recorded at the bottom of the column
592 rather than at the top as in the case of 5% CO₂. This is because most of the reaction happened
593 towards the top of the column and incoming lean solvent was heated by the outgoing, relatively
594 hot gas.

595 The poor performance of the absorber in this test could be due to the combination of the
596 following two reasons.

- 597 1. Solvent flow of 600 kg/h is too low for the absorption of CO₂ from the flue gas under
598 these operational and absorber design conditions.
- 599 2. The top of the absorber has pinched performance i.e. there is virtually no driving force
600 for absorbing any more CO₂. The phenomenon is referred to as chemical equilibrium
601 pinching [Brigman et al. 2014] i.e. if lean loading is not sufficiently low (solvent does
602 not have sufficient capacity), CO₂ equilibrium partial pressure in the lean stream
603 entering the absorber is close to the partial pressure of CO₂ in the gas leaving at the top
604 of the absorber. Under these conditions, mass transfer will drop in the upper section due
605 to lower mass transfer driving force available. In order to avoid such a situation, lean
606 loading should be dropped by increasing stripper temperature.

607 The bulge temperature further increased to 73 °C as the solvent flow rate increased to 1000kg/h
608 (Test 5) indicating an increase in absorption rate. However, the location of the bulge
609 temperature shifted downwards to 4.3m location. Again, the lowest temperature was recorded
610 at the top of the column due to shift of the reaction towards the lower part of the column. This
611 argument is also justified by around 15 °C increase in temperature at the bottom of the column
612 due to relatively hot solvent flowing down to the lower section of the column.

613 The bulge temperature stayed almost the same at 73 °C when flue gas flow rate was dropped to
614 150 m³/h (Test 6). It is interesting to note here that the cold part at the top of the column
615 elongated and second last temperature probe (5.6m) also measured temperature lower than the
616 bottom of the column. The bottom temperature further increased to close to the one measured
617 at 5.3m. Another interesting phenomenon noted here is that bottom 6 measurements are closer
618 as was the case in Test 3 while Tests 4 and 5 shown wider scattered temperature distribution.

619 As the solvent flow rate was increased to 1200 kg/h (Test 7), absorber temperatures shown an
620 interesting phenomenon. Bottom three temperatures shown an increase while rest of them
621 shown a drop. It is interesting that bottom four measurements recoded higher temperatures than
622 the top four. For the first time the bulge temperature recorded was in the lower half section of
623 the packing, at 2.9m, indicating that the reaction was shifted towards the lower section of the
624 column due to high liquid to gas ratio. Test 7 temperature profile indicates that the column is
625 pinched at the bottom, rich end. The rich end pinch occurs due to mass transfer limitations and
626 is independent of bulge temperature (Sachde *et al.*, 2014).

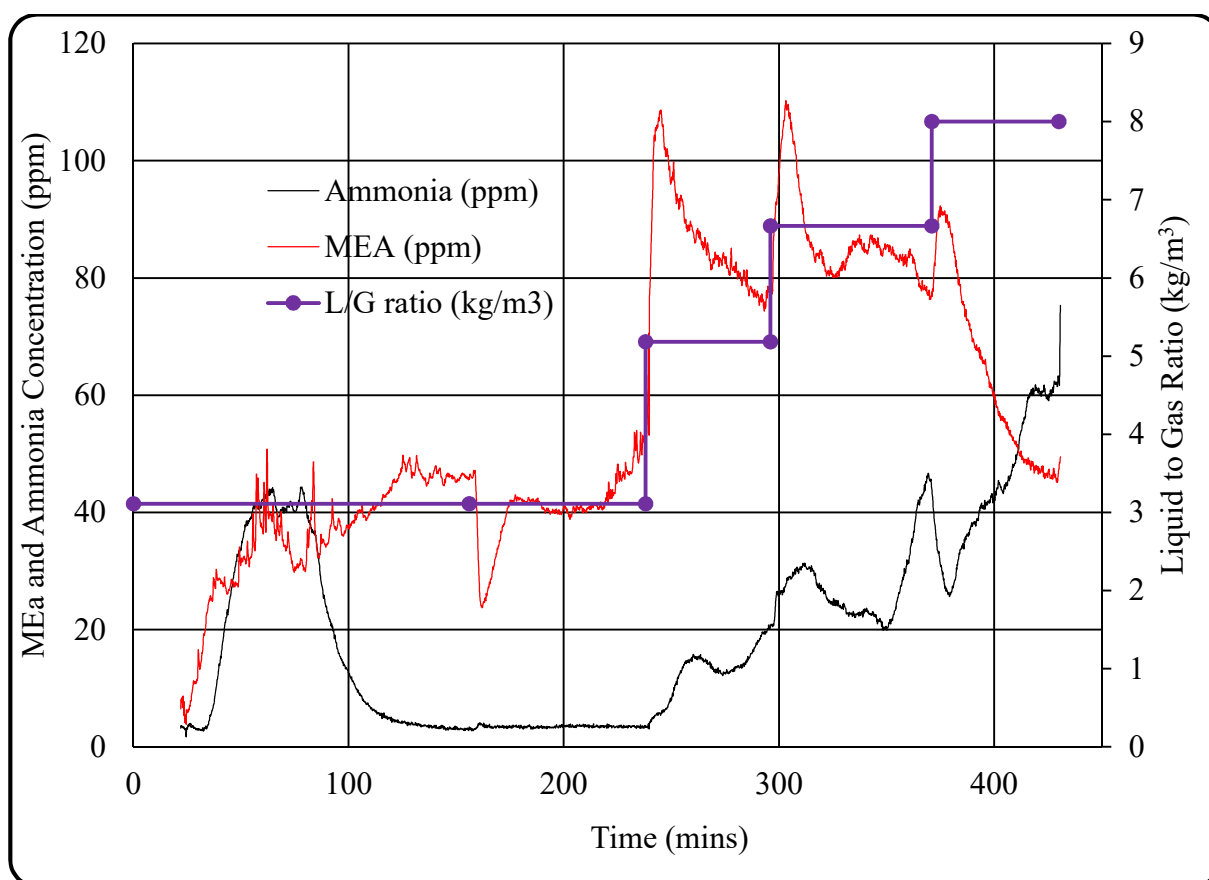
627 These observations indicate that absorber temperature profile is dependent on operational
628 conditions and that the bulge temperate shifts as the operational conditions are varied. So,
629 determination of the optimum location for solvent intercooling will be different for different
630 flue gas compositions, operational conditions and plant configurations and must be determined
631 on case by case basis. Moreover, the findings suggest that Raman Spectroscopy has the

632 capability to follow variations in process and can be employed for real time monitoring and
633 control of the CO₂ capture process.

634 Emissions:

635 Emissions of MEA and Ammonia as measured by FTIR at the outlet of the absorber are plotted
636 in Figure 13. The figure indicates that emissions are higher at higher L/G ratio (Tests 5-7) as
637 compared to those at low L/G ratio (Tests 3&4). Emissions of MEA were around 40 ppm during
638 low L/G ratio tests, but peaked to above 100 ppm for the higher L/G ratios. However, the water
639 wash has shown to remove most of the solvent from the gas before exiting to atmosphere.
640 Emissions of Ammonia, after initial peak at the startup, dropped to around 5ppm and stayed
641 low for low L/G ratios but started increasing as L/G gone up.

642



643

644 Figure 13: Emissions at the outlet of the absorber for process variation tests

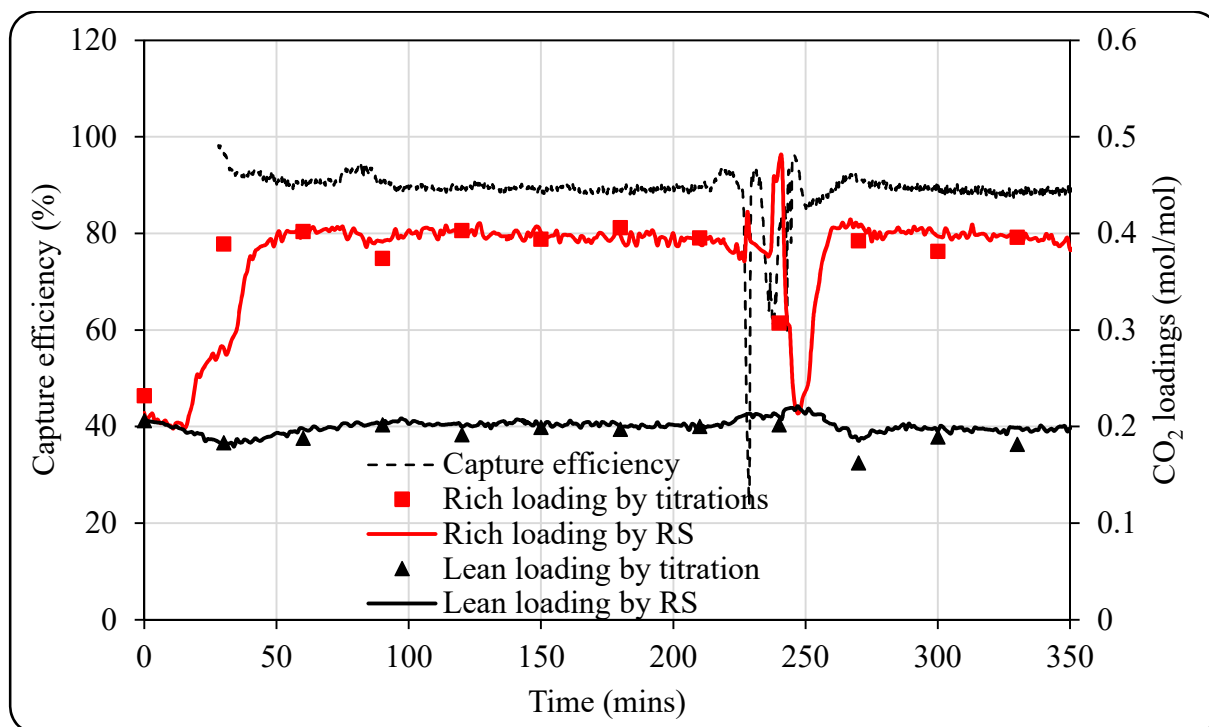
645

646 3.4 Coal Flue gas (with Sulphur dioxide)

647 For these tests, flue gas from a coal firing pulverized fuel combustor, containing 210 ppm of
648 SO₂ on average, was fed to the capture plant. The aim was to investigate if Raman
649 measurements are affected by solvent degradation. Operational condition for this test are given
650 in Table 4. Similarly to the previous cases, manual samples were taken from the plant and
651 titrated for CO₂ loadings and MEA concentration. Figure 14 compares Raman predictions with

652 titration results for rich and lean loadings. The real time Raman predictions and the offline
653 titration results show a satisfactory agreement throughout the entire process.

654 Rich loading drops sharply just after 200 mins of operation, see Figure 14, at this point the plant
655 was tripped and flue gas flow was ceased. The effect of plant trip is shown by drop in lean
656 loading after some time due to the reasons explained previously in this paper.



657

658 Figure 14: Comparison of rich and lean Raman measurements with titration data

659 The close agreement of Raman measurements with titration data provide evidence for the
660 accuracy of Raman predictions with respect to titration results. It can be concluded that the
661 presence or absence of SO₂ in the flue gas has not affected the CO₂ loading predictivity by the
662 Raman models which were developed based on partial least squares (PLS) algorithm.

663 Capture efficiency:

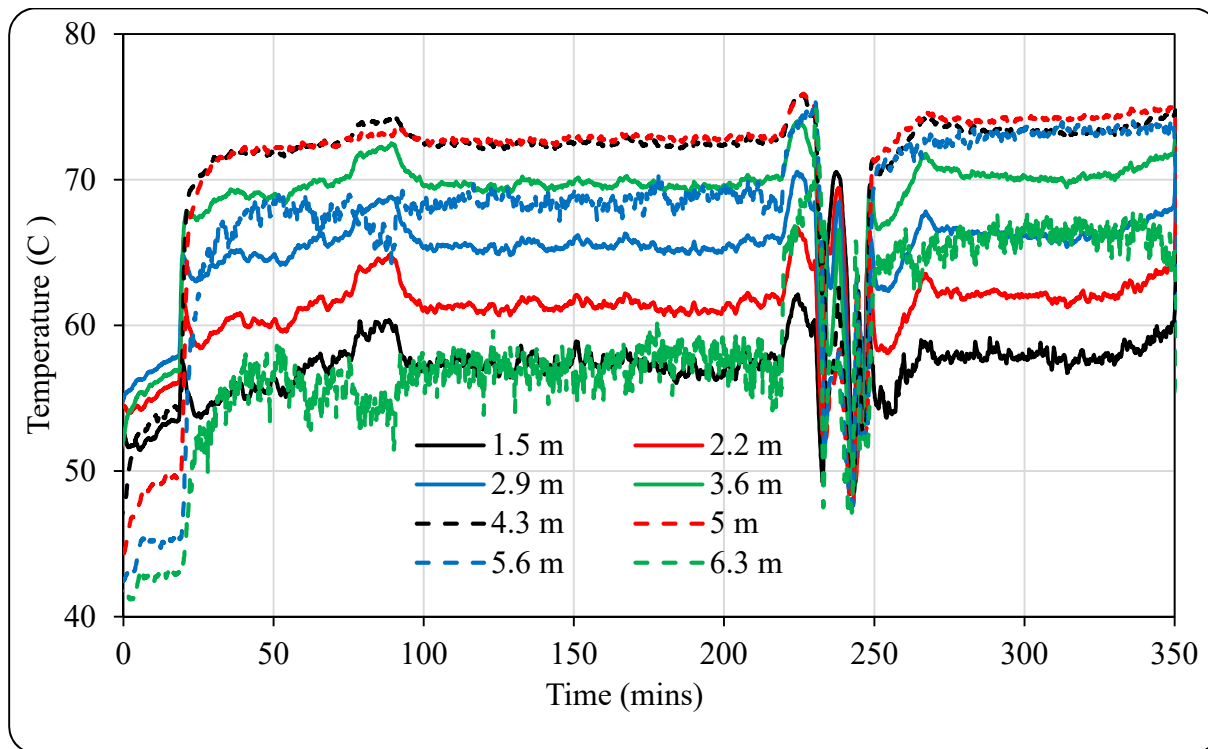
664 Figure 14 also plots capture efficiency as a function of time for tests with coal flue gas. The
665 plot shows that the capture efficiency was maintained around 90% throughout the test, except
666 when the plant has start/stop due to tripping. The same phenomenon is observed with rich and
667 lean Raman measurements, also plotted in Figure 14, where both the rich and lean loadings are
668 more or less unchanged.

669 Temperature profile:

670 Figure 15 shows absorber temperature profile for test with coal flue gas. It can be observed
671 from the plot that the highest temperature was measured at about 1/4th of the packing from the
672 top. The plot is showing temperature dips at around 2/3rd of the test period. As mentioned
673 previously, plant tripped at this point and all the flows stopped but was restarted promptly.

674 A close look at the temperature profile reveals that the temperature profile is different before
675 and after the plant has tripped. The reason for that is the change in temperature of lean solvent

676 entering the absorber. The temperature of the lean solvent was controlled at 40 °C and 50 °C,
677 before and after the plant trip, respectively. In both the cases, the temperature bulge is at almost
678 the same location but bulge temperature is little bit higher in the case of 50 °C. Moreover,
679 temperatures in the top half of the column are generally higher in the case of 50 °C lean solvent
680 temperature while those at the bottom of the column are not changed much.



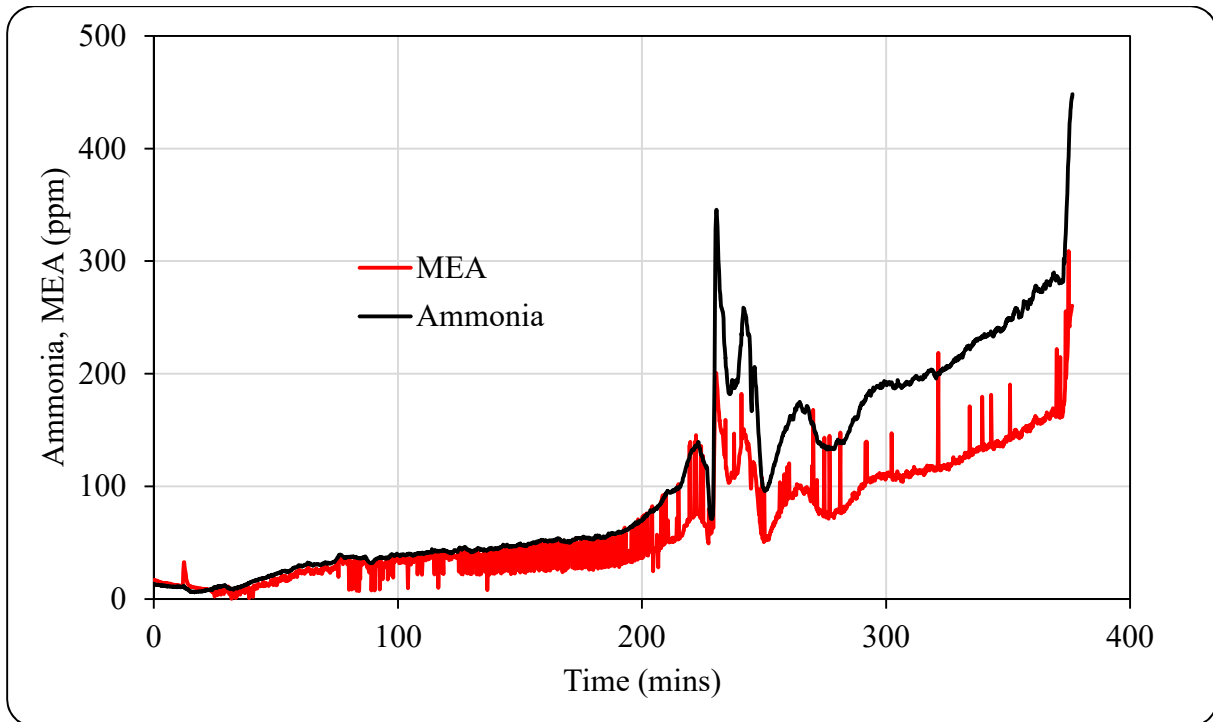
681

682

683 Figure 15: Absorber temperature profile for coal flue gas – temperature locations are from
684 bottom of the packing

685 Emissions:

686 Figure 16 plots emissions of ammonia and MEA at the exit of absorber for the coal flue gas
687 tests. It can be observed from the plot that emissions increased with time. This is due to the
688 persistent supply of 210 ppm of SO₂ in the flue gas resulting in degradation of solvent. The
689 continuous increasing trend in emissions indicate that solvent degradation rate was increasing.
690 The close agreement of Raman measurements with the offline titrations, even during
691 accelerated degradation, indicates that the Raman model developed here can be used to monitor
692 the capture plant performance.



693

694

Figure 16: Emissions during coal flue gas testing

695

4. Conclusions:

696 Solvent monitoring is very critical particularly in the case of dynamic CCS plant operation.
 697 Manual sampling is a labor-intensive task and has health and safety implications, including
 698 access to sampling points, harsh process conditions and chemical exposure. Moreover, it takes
 699 time to process samples and thus sampling frequency is reduced resulting in potentially losing
 700 critical data variations in the plant operation. There are several and complex mathematical and
 701 thermodynamic modeling developed to understand the CO₂ capture plant performance with
 702 respect to different process conditions in literature. Most of these models are limited to pen-
 703 and-paper due to the lack of validation with test results.

704 The Raman spectroscopic real time monitoring tool developed here is validated against pilot
 705 plant data in stable and dynamic conditions in both the absorption and desorption processes of
 706 CO₂ capture plant. Such a tool is one of most-awaited requirement in a CO₂ capture plant and
 707 its journey towards commercial deployment. The application of such a tool to the real time
 708 monitoring of capture plant can reduce the plant downtime, time and resources spending on
 709 offline analysis and provide the plant operator a better overview about the past-present plant
 710 conditions and ease to take decisions to optimize the plant operation. As Raman predictions can
 711 provide reliable real time measurements of rich and lean CO₂ loading at one-minute intervals,
 712 the validation of this analysis is apparent. Based on the tests carried out during these campaigns,
 713 following conclusions can be derived.

- 714 • Reliability of the Raman predictions are confirmed with the titration measurements
 715 carried out in this trial. Raman predictions can be mapped with the changes of process
 716 conditions and their intensities. They also provide information on stability of the plant.
- 717 • The Raman predictions models are not affected, with accelerated solvent degradation
 718 and increased emissions, during 180-235 ppm of SO₂ supply in the flue gas.

719 The test campaign at the PACT CO₂ capture plant with real time solvent monitoring using
720 Raman Spectroscopy has demonstrated that the technology is a step closer to making offline
721 measurements a thing of the past and moving towards predictive control of CO₂ capture plants.

722 **5. Acknowledgement:**

723 The authors would like to acknowledge the financial support of the UK Carbon Capture and
724 Storage Research Centre and PhD scholarship funded by University of South-Eastern Norway
725 for carrying out this research work. The authors also acknowledge that the PACT Facilities
726 (<https://pact.group.shef.ac.uk>), funded by the Department for Business, Energy and Industrial
727 Strategy and the EPSRC, have been used for the research work reported in this publication.

728 **6. References:**

729 Abu-Zahra, M.R.M., Schneiders L.H.J., Niederer J.P.M., Feron P.H.M., Versteeg G.F.,
730 (2007). CO₂ capture from power plants: Part I. A parametric study of the technical
731 performance based on monoethanolamine, *International Journal of Greenhouse Gas*
732 *Control*, Volume 1, Issue 1, April 2007, Pages 37-46.

733 Ahn, H., Luberti, M., Liu, Z., Brandani, S., (2013). Process configuration studies of the
734 amine capture process for coal-fired power plants. *Int. J. Greenh. Gas Control* 16: 29–40.

735 Akram M., Ali U., Best T., Blakey S., Finney, K.N., Pourkashanian M., (2016).
736 Performance evaluation of PACT Pilot-plant for CO₂ capture from gas turbines with
737 Exhaust Gas Recycle, *International Journal of Greenhouse Gas Control*, Volume 47, April
738 2016, Pages 137-150.

739 Amrollahi, Z., Ertesvag, I.S., Bolland, A., (2011). Optimized process configurations of
740 post-combustion CO₂ capture for natural-gas-fired power plant-exergy analysis. *Int. J.*
741 *Greenh. Gas Control* 5: 1393–1405.

742 Andersson, V., Wittmeyer, K., Gorset, O., Maree, Y., & Sanden, K. (2013). Operational
743 Experience and Initial Results from the First Test Period at CO₂ Technology Centre
744 Mongstad. *Energy Procedia*, 37, 6348-6356. <https://doi.org/10.1016/j.egypro.2013.06.564>

745 Aronu, U.E., Svendsen H.F., and Hoff, K.A., (2010). Investigation of amine amino acid
746 salts for carbon dioxide absorption. *International Journal of Greenhouse Gas Control*, 2010.
747 4: 771-775.

748 BEIS Committee Report, (2019). Carbon Capture usage and storage: Third time lucky,
749 Twentieth report of Session 2017-19, 25th April 2019.

750 Cheng H., Lai C., Tan C. (2013). Thermal regeneration of alkanolamine solutions in a
751 rotating packed bed. *Int J Greenhouse Gas Control* 16: 206–16.

752 Clean Growth, (2018). The UK Carbon Capture Usage and Storage deployment pathway-
753 An action Plan, 2018.

754 Da Silva, E.F., Lepaumier, H., Grimstvedt, A., Vevelstad, S.J., Einbu, A., Vernstad, K.,
755 Svendsen, H.F., Zahlsen, K., (2012). Understanding 2-Ethanolamine Degradation in
756 Postcombustion CO₂ Capture. *Ind. Eng. Chem. Res.* 2012, 51, 13329–13338.

757 de Cazenove T., Bouma RHB., Goetheer ELV., van Os PJ. and Hamborg ES., (2016).
758 “Aerosol measurement technique: Demonstration at CO₂ Technology Centre Mongstad.”
759 Energy Proc 86:160–170.

760 Diego ME., Akram M., Bellas JM., Finney KN. and Pourkashanian M. (2017). Making gas-
761 CCS a commercial reality: The challenges of scaling up. Greenhouse Gases: Science and
762 Technology 7 (5): 778-807.

763 Einbu, A., Ciftja, A. F., Grimstvedt, A., Zakeri, A., & Svendsen, H. F. (2012). Online
764 analysis of amine concentration and CO₂ loading in MEA solutions by ATR-FTIR
765 spectroscopy. Energy Procedia, 23, 55-63. <https://doi.org/10.1016/j.egypro.2012.06.040>

766 Esbensen, K. H., Guyot, D., Westad, F., Houmoller, L.P. (2010). Multivariate data analysis:
767 in practice: CAMO Software

768 Flø, N. E., Faramarzi, L., de Cazenove, T., Hvidsten, O. A., Morken, A. K., Hamborg, E.
769 S., Gjernes, E. (2017). Results from MEA Degradation and Reclaiming Processes at the
770 CO₂ Technology Centre Mongstad. Energy Procedia, 114, 1307-1324.
771 <https://doi.org/10.1016/j.egypro.2017.03.1899>

772 Hakka, L., (2007). Cansolv Technologies Inc. 2007, private communication.

773 Herraiz L., (2016). Selective Exhaust Gas Recirculation in Combined Cycle Gas Turbine
774 Power Plants with Post-combustion Carbon Capture. PhD Thesis. University of Edinburgh,
775 Scotland, UK.

776 Idris, Z., Jens, K. J., & Eimer, D. A. (2014). Speciation of MEA-CO₂ Adducts at
777 Equilibrium Using Raman Spectroscopy. Energy Procedia, 63, 1424-1431.
778 <https://doi.org/10.1016/j.egypro.2014.11.152>

779 Jassim, M.S., Rochelle G., Eimer D. and Ramshaw C., (2007). Carbon dioxide absorption
780 and desorption in aqueous monoethanolamine solutions in a rotating packed bed. Industrial
781 & Engineering Chemistry Research, 2007. 46: 2823-2833.

782 Jinadasa, M. H. W. N. (2019). Process analytical technology for real-time quantitative
783 speciation of aqueous phase CO₂ capture solvents. (PhD thesis), University of South-
784 Eastern Norway, Porsgrunn. (ISBN: 978-82-7206-523-1)

785 Jinadasa, M. H. W. N., Jens, K.-J., & Halstensen, M. (2018). Process Analytical Technology
786 for CO₂ Capture. In Karamé, I., Shaya, J., & Srour, H. (Eds.), Carbon Dioxide Chemistry,
787 Capture and Oil Recovery: Intech Open. DOI: 10.5772/intechopen.76176

788 Jinadasa, M. H. W. N., Jens, K.-J., Øi, L. E., & Halstensen, M. (2017). Raman spectroscopy
789 as an online monitoring tool for CO₂ capture process: Demonstration using a laboratory rig.
790 Energy Procedia, 114, 1179-1194. <https://doi.org/10.1016/j.egypro.2017.03.1282>

791 Kachko, A. (2016). In-line monitoring of solvents during CO₂ absorption using multivariate
792 data analysis. (PhD thesis), Technische Universiteit Delft, (ISBN: 978-94-6186-673-8)

793 Kachko, A., van der Ham, L. V., Bakker, D. E., van de Runstraat, A., Nienoord, M., Vlugt,
794 T. J. H., & Goetheer, E. L. V. (2016a). In-Line Monitoring of the CO₂, MDEA, and PZ
795 Concentrations in the Liquid Phase during High Pressure CO₂ Absorption. Industrial &
796 Engineering Chemistry Research, 55(13), 3804-3812. 10.1021/acs.iecr.6b00141

797 Kachko, A., van der Ham, L. V., Bardow, A., Vlught, T. J. H., & Goetheer, E. L. V. (2016b).
798 Comparison of Raman, NIR, and ATR FTIR spectroscopy as analytical tools for in-line
799 monitoring of CO₂ concentration in an amine gas treating process. *International Journal of*
800 *Greenhouse Gas Control*, 47, 17-24. <https://doi.org/10.1016/j.ijggc.2016.01.020>

801 Kachko, A., van der Ham, L. V., Geers, L. F. G., Huizinga, A., Rieder, A., Abu-Zahra, M.
802 R. M., Goetheer, E. L. V. (2015). Real-Time Process Monitoring of CO₂ Capture by
803 Aqueous AMP-PZ Using Chemometrics: Pilot Plant Demonstration. *Industrial &*
804 *Engineering Chemistry Research*, 54(21), 5769-5776. 10.1021/acs.iecr.5b00691

805 Kang J.L., Wong D.S.H., Jang S.S., and Tan C.S., (2016). A comparison between packed
806 beds and rotating packed beds for CO₂ capture using monoethanolamine and dilute aqueous
807 ammonia solutions. *International Journal of Greenhouse Gas Control*, 2016. 46: 228-239.

808 Kim, Y.E., Lim, J.A., Jeong, S.K., Yoon, Y.I., Bae, S.T., Nam, S.C., (2013). Comparison
809 of carbon dioxide absorption in aqueous MEA, DEA, TEA and AMP solutions. *Bulletin of*
810 *Korean Chemical Society* 34: 783–787.

811 Knudsen, J.N., Jensen, J.N., Vilhelmsen, P.J., Biede, O., (2007). First year operation
812 experience with a 1 t/h CO₂ absorption pilot plant at Esbjerg coal-fired power plant. In
813 *Proceedings of the European Congress of Chemical Engineering (ECCE-6)*, Copenhagen,
814 Denmark, 16–20 September 2007.

815 Kohl, A.L., Nielsen, R.B., (1997). *Gas Purification*, 5th ed.; Gulf Professional Publishing:
816 Houston, TX, USA, 1997.

817 Kumar, S., Cho J.H. and Moon I., Ionic liquid-amine blends and CO₂ BOLs (2014).
818 Prospective solvents for natural gas sweetening and CO₂ capture technology – A review.
819 *International Journal of Greenhouse Gas Control*, 2014. 20: 87-116.

820 Le Moullec Y., Neveux T., Al Azki A., Chikukwa A. and Hoff KA., (2014). Process
821 modifications for solvent-based post-combustion CO₂ capture. *Int J Greenhouse Gas*
822 *Control* 31: 96–112.

823 Lepaumier, H., Da Silva, E.F., Einbu, A., Grimstvedt, A., Knudsen, J.N., Zahlsen, K.,
824 Svendsen, H.F., (2011). Comparison of MEA degradation in pilot-scale with lab-scale
825 experiments. *Energy Procedia* 2011, 4, 1652–1659.

826 Madan, T., Sachde, D., Lin, Y.-J., Frailie, P., Rochelle, G.T., (2013). Improved process
827 configurations for amine scrubbing. In: *7th Trondheim Conference on CO₂ Capture,*
828 *Transport and Storage*, Trondheim (NO), 4–6 June.

829 Mejdell T. Vassbotn T. Juliussen O., et al. (2011). “Novel full height pilot plant for solvent
830 development and model validation.” *Energy Procedia* 4:1753–1760.

831 Merkel TC. Wei X., He Z., White LS. Wijmans JG. Baker RW. (2013). Selective exhaust
832 gas recycle with membranes for CO₂ capture from natural gas combined cycle power plants.
833 *Ind Eng Chem Res* 52:1150–1159 (2013).

834 Montañés, R. M., Flø, N. E., Dutta, R., Nord, L. O., & Bolland, O. (2017). Dynamic Process
835 Model Development and Validation with Transient Plant Data Collected from an MEA Test

836 Campaign at the CO₂ Technology Center Mongstad. *Energy Procedia*, 114, 1538-1550.
837 <https://doi.org/10.1016/j.egypro.2017.03.1284>

838 Notz R, Mangalapally HP. and Hasse H. (2012). “Post combustion CO₂ capture by reactive
839 absorption: Pilot plant description and results of systematic studies with MEA.” *Int J*
840 *Greenhouse Gas Control* 6: 84–112.

841 Oh SY. Yun S. Kim JK. (2018). Process integration and design for maximizing energy
842 efficiency of a coal fired power plant integrated with amine-based CO₂ capture process.
843 *Applied Energy* 216:311–322.

844 Polasek, J. and Bullin J.A., (2006). *Selecting Amines for Sweetening Units*, Bryan Research
845 and Engineering, Inc. - Technical Papers, 2006.

846 Puxty, G., Bennett, R., Conway, W., & Maher, D. (2016). A comparison of Raman and IR
847 spectroscopies for the monitoring and evaluation of absorbent composition during CO₂
848 absorption processes. *International Journal of Greenhouse Gas Control*, 49, 281-289.
849 <https://doi.org/10.1016/j.ijggc.2016.03.012>

850 Reynolds, A. J., Verheyen, T. V., Adeloju, S. B., Chaffee, A. L., & Meuleman, E. (2015).
851 Evaluation of methods for monitoring MEA degradation during pilot scale post-combustion
852 capture of CO₂. *International Journal of Greenhouse Gas Control*, 39, 407-419.
853 <https://doi.org/10.1016/j.ijggc.2015.06.001>

854 Rochelle, G.T., (2012). Thermal degradation of amines for CO₂ capture. *Curr. Opin. Chem.*
855 *Eng.* 2012, 1, 183–190.

856 Sachde, D., & Rochelle, G. T., (2014). Absorber Intercooling Configurations using
857 Aqueous Piperazine for Capture from Sources with 4 to 27% CO₂. *Energy Procedia*, 63,
858 1637-1656. <https://doi.org/10.1016/j.egypro.2014.11.174>

859 Souchon, V., Aleixo, M. d. O., Delpoux, O., Sagnard, C., Mougin, P., Wender, A., &
860 Raynal, L. (2011). In situ determination of species distribution in alkanolamine- H₂O-CO₂
861 systems by Raman spectroscopy. *Energy Procedia*, 4, 554-561.

862 Tait, P., Buschle, B., Milkowski, K., Akram, M., Pourkashanian, M., & Lucquiaud, M.
863 (2018). Flexible operation of post-combustion CO₂ capture at pilot scale with demonstration
864 of capture-efficiency control using online solvent measurements. *International Journal of*
865 *Greenhouse Gas Control*, 71, 253-277. <https://doi.org/10.1016/j.ijggc.2018.02.023>

866 Van der Ham, L.V., van Eekveld, A.C., & Goetheer, E.L.V., (2014). Online Monitoring
867 of Dissolved CO₂ and MEA Concentrations: Effect of Solvent Degradation on Predictive
868 Accuracy. *Energy Procedia*, 63, 1223-1228. <https://doi.org/10.1016/j.egypro.2014.11.132>

869 Vogt, M., Pasel, C., & Bathen, D. (2011). Characterisation of CO₂ absorption in various
870 solvents for PCC applications by Raman spectroscopy. *Energy Procedia*, 4, 1520-1525.
871 <https://doi.org/10.1016/j.egypro.2011.02.020>

872 Wang M., Joel AS., Ramshaw C., Eimer D., Musa NM. (2015). Process intensification for
873 post-combustion CO₂ capture with chemical absorption: A critical review. *Applied Energy*
874 158: 275–291.

875 Wong, M. K., Shariff, A. M., & Bustam, M. A. (2015). Chemical speciation of CO₂
876 absorption in aqueous monoethanolamine investigated by in situ Raman spectroscopy.
877 International Journal of Greenhouse Gas Control, 39, 139–147.
878 <https://doi.org/10.1016/j.ijggc.2015.05.016>

879 Wong, M. K., Shariff, A. M., & Bustam, M. A. (2016). Raman spectroscopic study on the
880 equilibrium of carbon dioxide in aqueous monoethanolamine. RSC Advances, 6(13),
881 10816-10823. 10.1039/C5RA22926J

882 Xie, H.-B., Zhou, Y., Zhang, Y., & Johnson, J. K. (2010). Reaction Mechanism of
883 Monoethanolamine with CO₂ in Aqueous Solution from Molecular Modeling. The Journal
884 of Physical Chemistry A, 114(43), 11844-11852. 10.1021/jp107516k

885 Yang Q., Puxty G., James S., Bown M., Feron P., Conway W., (2016). Toward Intelligent
886 CO₂ Capture Solvent Design through Experimental Solvent Development and Amine
887 Synthesis. Energy Fuels 30: 7503–7510.

888 Yuan Y. and Rochelle G.T., (2018). CO₂ absorption rate in semi-aqueous
889 monoethanolamine. Chemical Engineering Science, 2018. 182: 56-66.

890

891

892